Kidney International, Vol. 66 (2004), pp. 586–590

DNAzyme for TGF-β suppressed extracellular matrix accumulation in experimental glomerulonephritis

YOSHITAKA ISAKA, HIROYUKI NAKAMURA, MASAYUKI MIZUI, YOSHITSUGU TAKABATAKE, MASARU HORIO, HIROSHI KAWACHI, FUJIO SHIMIZU, ENYU IMAI, and MASATSUGU HORI

Department of Internal Medicine and Therapeutics, Osaka University Graduate School of Medicine, Osaka, Japan; Department of Clinical Laboratory Science, Osaka University Graduate School of Medicine, Osaka, Japan; and Institute of Nephrology, Niigata University School of Medicine, Asahimachi-dori, Niigata, Japan

DNAzyme for TGF-β suppressed extracellular matrix accumulation in experimental glomerulonephritis.

Background. We developed an electroporation-mediated gene transfer method targeting glomerular mesangial cells. Injecting DNA solution via renal artery followed by electric pulses using tweezers-type electrodes could result in efficient transfection in mesangial cells. Therefore, this gene transfer system opened a feasible strategy to manipulate the function of several cytokines and growth factors in mesangial cells. Recently, a new generation of catalytic nucleic acid composed of DNA, named DNA enzyme (DNAzyme), has been developed.

Method. We generated a DNAzyme (TGFDE) targeting transforming growth factor-β1 (TGF-β1), and examined the therapeutic effect of TGFDE in vitro and in vivo.

Results. In cultured rat mesangial cells, treatment with TGFDE blocked TGF-β1 mRNA expression, and thereby suppressed type I collagen mRNA expression. Next, we introduced TGFDE or scrambled DNAzyme (TGFSCR) into anti-Thy-1 model of nephritic rats by electroporation 3 days after disease induction. Northern blot analysis and immunohistochemical staining demonstrated that glomerular message and protein expression of TGF-β1, α-smooth muscle actin (α-SMA), and type I collagen were suppressed in TGFDE-transfected nephritic rats compared with untreated nephritic rats and TGFSCR-transfected rats on day 7. Consequently, we observed significant reduction in glomerular matrix score in TGFDE-transfected nephritic rats.

Conclusion. Inhibition of TGF-β1 expression by electroporation-mediated DNAzyme transfer might be useful for the therapy of glomerulonephritis.

Glomerular mesangial cell proliferation and extracellular matrix (ECM) accumulation are central features of numerous experimental and human glomerular diseases. These processes are thought to play an important role in the development of glomerulosclerosis and renal failure. Transforming growth factor-β (TGF-β) regulates biologic processes such as cell proliferation, differentiation, and immunologic reaction. One of the most important biologic actions of TGF-β is the regulation of ECM accumulation [1]. Previous reports strongly suggest that the inhibition of mesangial TGF-β expression should be one of the crucial therapeutic strategies to prevent the progression of renal fibrosis.

Recently, we developed a new gene transfer system by electroporation in vivo; infusing DNA solution via renal artery followed by electric pulses using tweezers-type electrode could introduce genes into mesangial cells in almost all of the glomeruli [2]. Electroporation is free from oncogenicity, immunogenicity, and cytotoxicity of viral vectors. In addition, electroporation-mediated gene transfer technique resulted in significantly higher transfection efficiency than hemaglutinating virus of Japan (HVJ) liposome method [2].

A new generation of catalytic nucleic acid composed of DNA, named DNAzyme, has been developed. These DNAzymes can potentially cleave RNA at any purine-pyrimidine junction and offer greater substrate specificity than hammerhead ribozymes [3, 4]. This study examined whether electroporation-mediated DNAzyme transfer could inhibit the TGF-β1 action in mesangial cells in vivo.

METHODS

Design of DNAzyme

Sequences of DNAzyme (TGFDE) for rat TGF-β1 used in the present study were 5′-CGAGGGCGGCAG GCTAGCTACAACGAGGGGGAGGC*T*-3′ (3′ thymidine inverted is italic, catalytic domain is underlined) (Bex, Tokyo, Japan). TGFDE has nine and eleven nucleotide arms flanking the 15 nucleotide catalytic domain (underlined), which was designed to target the translational site adenine-uracil-guanine (AUG) in rat TGF-β1 mRNA. For resistance to 3′-to-5′ exonuclease

Key words: DNAzyme, electroporation, TGF-β, gene therapy.

Received for publication July 14, 2003
and in revised form December 29, 2003, and February 9, 2004
Accepted for publication February 20, 2004

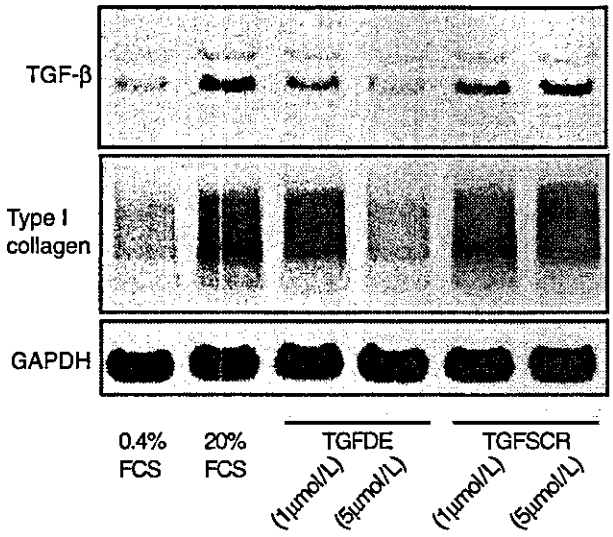

Fig. 1. The effect of DNAzyme in cultured rat mesangial cells. Northern blot analysis demonstrated DNAzyme, TGFDE, blocked fetal calf serum (FCS)-induced transforming growth factor-β1 (TGF-β1) and type I collagen expression, while scrambled oligonucleoside, TGFSCR, had no effect. GAPDH is glyceraldehyde-3-phosphate dehydrogenase.

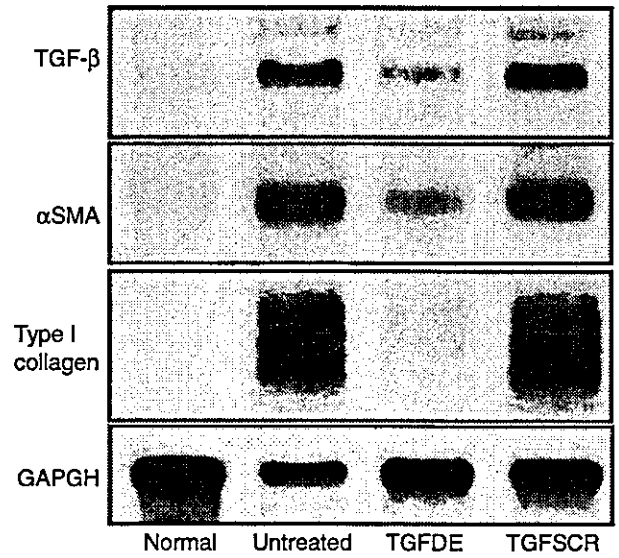

Fig. 2. Inhibition of transforming growth factor-β1 (TGF-β1), α-smooth muscle actin (α-SMA), and type I collagen mRNA in nephritic glomeruli by TGFDE. RNA was extracted from isolated glomeruli of normal kidney or untreated, TGFDE-treated and TGFSCR-treated nephritic kidney. Northern blot was probed for TGF-β1, αSMA, type I collagen, or glyceraldehyde-3-phosphate dehydrogenase (GAPDH).

digestion, the 3′ terminus of the molecule was capped with an inverted 3′-3′-linked thymidine (italics). The nucleotide sequence in each arm of TGFDE was scrambled without altering the catalytic domain (TGFSCR). TGFSCR sequences were 5′-GGGGGAGGCGGCTAG CTACAACGACGAGGGCGGCA*T*-3′ (3′ thymidine inverted is italic, catalytic domain is underlined).

Effects of TGFDE in cultured mesangial cells

To examine the effects of TGFDE on TGF-β1 and type I collagen expression on mesangial cells, subconfluent rat mesangial cells [5] were growth arrested with 0.4% fetal calf serum (FCS). Quiescent subconfluent cells were treated with adding TGFDE or TGFSCR (1 and 5 μmol/L) for 24 hours. Treated cells were then stimulated with 20% FCS for 8 hours and TGF-β1 and type I collagen mRNA expression was determined by Northern blot analysis. TGFDE blocked FCS-induced TGF-β1 and type I collagen mRNA expression on rat mesangial cells, while TGFSCR had no effect (Fig. 1).

Experimental design in anti-Thy-1 nephritis

To determine the therapeutic effect of TGFDE on mesangial proliferative glomerulonephritis, we transferred TGFDE into nephritic rats by electroporation in vivo [2]. All procedures were handled in a humane fashion in accordance with the guidelines of the Animal Committee of Osaka University. Six-week-old male Sprague-Dawley rats were anesthetized by intraperitoneal injection of pentobarbital (50 mg/kg) and anti-Thy-1 model of glomerulonephritis was induced by an intravenous injection of anti-Thy-1 monoclonal antibody, 1-22-3 (5 mg/kg) [6]. On day 3, TGFDE or TGFSCR (200 μg) was transferred into nephritic rats (four rats in each group).

On day 7, treated left kidneys and untreated contralateral right kidneys were perfused with cold autoclaved phosphate-buffered saline (PBS), and samples of tissues for light microscopy were fixed with 4% paraformaldehyde overnight and dehydrated through a graded ethanol series and embedded in paraffin. Histologic sections (2 μm) of the kidneys were stained with periodic acid-Schiff (PAS) reagent. Tissues for α-smooth muscle actin (α-SMA) immunostaining were fixed in methyl Carnoy's solution. For glomerular RNA preparations, glomeruli were isolated from the pooled remaining renal tissue by a standard sieving method. The experiments were repeated three times.

RESULTS

Effect of TGFDE on TGF-β α-SMA and collagen I expression in vivo

To examine the effects of TGFDE in vivo, we transferred TGFDE or TGFSCR into nephritic rats on day 3, and examined glomerular mRNA levels on day 7. Northern blot analysis demonstrated that TGF-β1 mRNA levels were markedly increased in untreated and TGFSCR-treated nephritic kidneys. In contrast, TGFDE transfection reduced the levels of TGF-β1 mRNA. In addition, glomerular mRNA levels of α-SMA and type I collagen were increased in untreated and TGFSCR-treated kidneys, while TGFDE transfection inhibited the α-SMA and type I collagen expression (Fig. 2). Laser

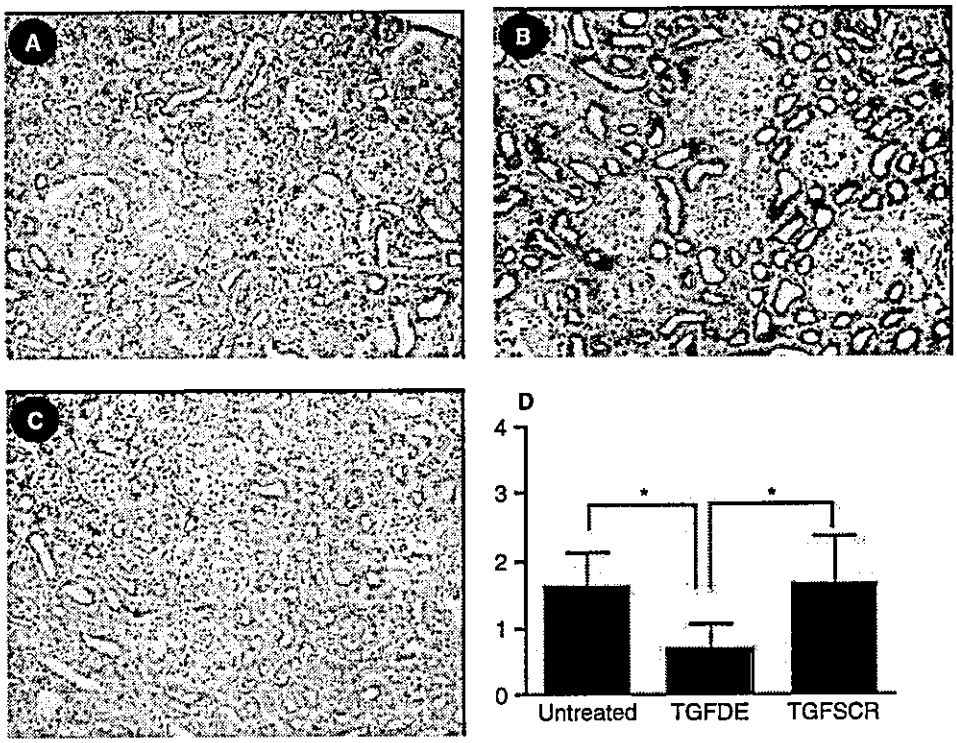

Fig. 3. Inhibition of glomerular expression of transforming growth factor-β (TGF-β) by TGFDE. Representative photomicrographs show the immunohistochemical staining for TGF-β in untreated (*A*), TGFDE-treated (*B*), and TGFSCR-treated (*C*) nephritic kidney (×200). TGFDE (*D*) significantly suppressed glomerular TGF-β expression (1.69 ± 0.49, 0.81 ± 0.47, and 1.73 ± 0.63 in untreated, TGFDE, and TGFSCR, respectively). $^*P < 0.001$.

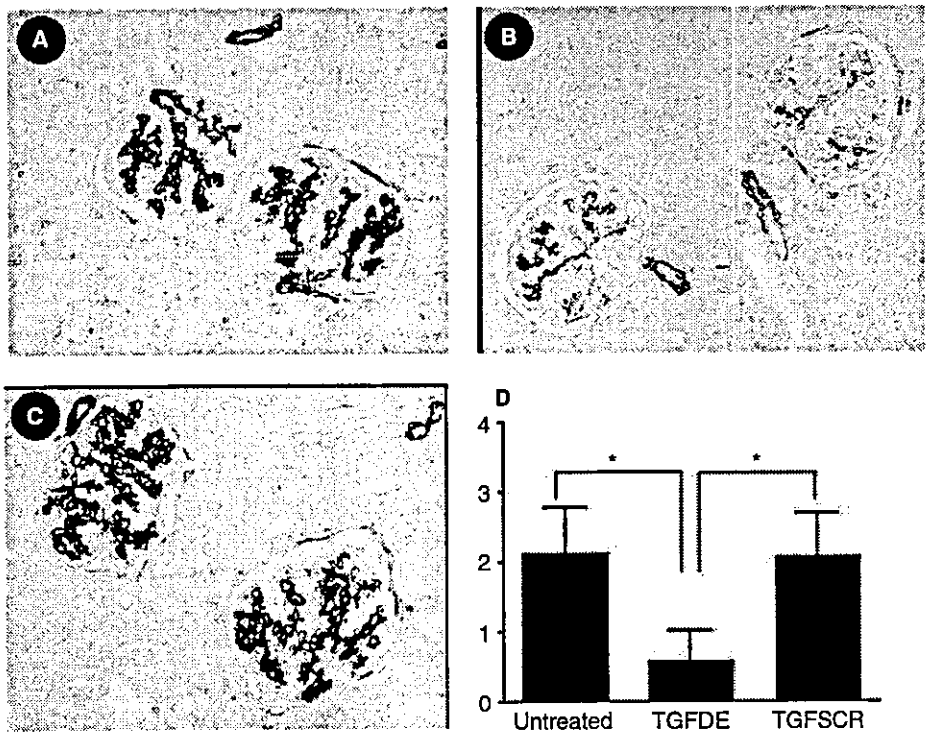

Fig. 4. Inhibition of glomerular expression of α-smooth muscle actin (α-SMA) by TGFDE. Representative photomicrographs show the immunohistochemical staining for α-SMA in untreated (*A*), TGFDE-treated (*B*), and TGFSCR-treated (*C*) nephritic kidney (×200). TGFDE (*D*) significantly suppressed glomerular α-SMA expression (2.17 ± 0.72, 0.72 ± 0.42, and 2.14 ± 0.66 in untreated, TGFDE, and TGFSCR, respectively). $^*P < 0.001$.

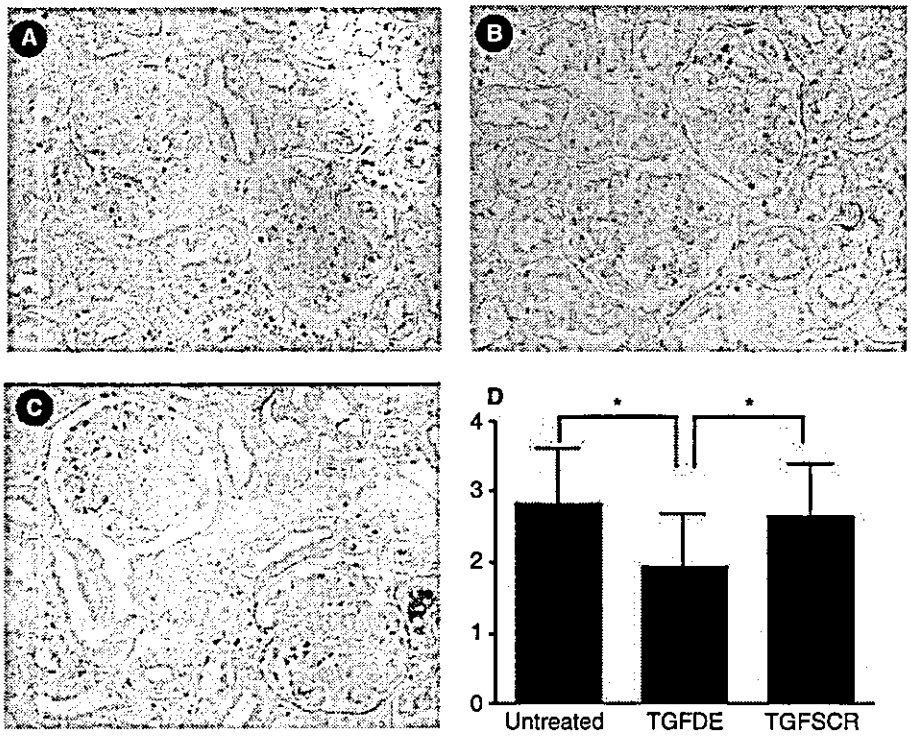

Fig. 5. Inhibition of glomerular extracellular matrix (ECM) accumulation by TGFDE. Representative photomicrographs show periodic acid-Schiff (PAS) staining in untreated (*A*), TGFDE-treated (*B*), and TGFSCR-treated (*C*) nephritic kidney (×200). Glomerular matrix score (*D*) was significantly reduced in TGFDE-treated kidneys compared with untreated and TGFSCR-treated kidneys (2.85 ± 0.78, 1.97 ± 0.72, and 2.68 ± 0.73 in untreated, TGFDE, and TGFSCR, respectively). $^*P < 0.001$.

densitometric analysis revealed that TGF-β1 and type I collagen mRNA in glomeruli from nephritic rats treated with TGFDE was reduced to 47% and 34% of those in untreated disease control, respectively.

TGF-β1 (Fig. 3) and αSMA (Fig. 4) protein expression was studied by immunohistochemistry using antihuman TGF-β1 polyclonal antibody (Santa Cruz Biotechnology, Santa Cruz, CA, USA) and anti-α-SMA monoclonal antibody (Immunotech, Marseilles, France), respectively. Expression of TGF-β1 was up-regulated in the glomeruli from nephritic rats, and this expression was significantly suppressed in those rats treated with TGFDE (Fig. 3D). In contrast, the level of TGF-β1 expression was unchanged in TGFSCR-treated rats. We also observed α-SMA expression in the glomeruli of untreated and TGFSCR-treated kidneys. However, immunostaining of α-SMA was significantly weak in TGFDE-treated kidney (Fig. 4D).

DISCUSSION

Effect on glomerular matrix accumulation

To determine the effect on the histological changes in nephritic kidneys, histologic analysis was performed using PAS staining. PAS staining showed marked ECM accumulation in untreated and TGFSCR-treated kidneys. In contrast, TGFDE transfection reduced ECM accumulation (Fig. 5). The degree of glomerular matrix accumulation was determined as the percentage of each glomerulus occupied by mesangial matrix. Glomerular matrix score was significantly reduced in TGFDE-treated kidneys compared with untreated and TGFSCR-treated kidneys. We further examined the effect of TGFDE on glomerular platelet-derived growth factor (PDGF) expression by reverse transcription-polymerase chain reaction (RT-PCR), and observed no differences between three groups (data not shown). In addition, glomerular cell number was not affected (79.5 ± 9.7, 75.9 ± 8.2, and 80.6 ± 9.3 in untreated, TGFDE, and TGFSCR, respectively). TGF-β is considered necessary for the glomerular remodeling. We examined the healing process of mesangiolysis and the later stage of the disease in the treated rats. TGFDE transfection did not interfere with the initial injury in the anti-Thy-1 model, because treated and untreated kidney had equivalent mesangiolysis. On the contrary, the healing process seemed accelerated in TGFDE-treated kidney probably due to the suppression of excessive ECM deposition.

In order to inhibit the gene expression by cleavage of the target mRNA, antisense oligonucleotides has been adopted [7]. We compared the effect of TGFDE with antisense oligonucleotides. Treatment with antisense

oligonucleotide (200 μg) for TGF-β1 also reduced glomerular TGF-β1 and type I collagen mRNA expression to 53% and 41% of untreatment, respectively. TGFDE was not less effective than antisense oligonucleotides in treating nephritic disease was consistent with the previous report [4]. However, the effect of antisense may be transient, because RNase H bases antisense mechanism on the hydrolysis of RNA-DNA duplex [8]. In contrast, the 3′ terminus of TGFDE was capped with an inverted 3′-3′-linked thymidine for resistance to 3′-to-5′ exonuclease digestion, because phosphorothioate modified oligonucleotides may hamper the cellular function [4].

We should establish the safety of this method prior to clinical application. However, we observed no damage in glomeruli and tubular epithelial cells when TGFDE was transferred into normal kidney on histologic examination. In addition, there was no difference between normal and TGFDE-treated rats in the serum lactate dehydrogenase (LDH) levels (117.5 ± 26.7 and 129.3 ± 29.2 in untreated and TGFDE, respectively), suggesting no major toxicity of electroporation-mediated TGFDE transfer.

CONCLUSION

Our study demonstrates that DNA injection via renal artery followed by electroporation could be a powerful therapeutic tool in vivo. The molecular intervention by DNAzyme for TGF-β may be a promising strategy for treatment of glomerular diseases.

Reprint requests to Yoshitaka Isaka, M.D, Ph.D., Department of Internal Medicine and Therapeutics, Osaka University Graduate School of Medicine, Suita 565–0871, Osaka, Japan.
E-mail: isaka@medone.med.osaka-u.ac.jp

REFERENCES

1. Border W, Noble N: Transforming growth factor in tissue fibrosis. *N Engl J Med* 331:1286–1292, 1994
2. Tsujie M, Isaka Y, Nakamura H, *et al*: Electroporation-mediated gene transfer that targets glomeruli. *J Am Soc Nephrol* 12:949–954, 2001
3. Santoro SW, Joyce GF: A general purpose RNA-cleaving DNA enzyme. *Proc Natl Acad Sci USA* 94:4262–4266, 1997
4. Santiago F, Lowe H, Kavurma M, *et al*: New DNA enzyme targeting Egr-1 mRNA inhibits vascular smooth muscle proliferation and regrowth after injury. *Nat Med* 5:1264–1269, 1999
5. Sugiura T, Wada A, Itoh T, *et al*: Group II phospholipase A_2 activates mitogen-activated protein kinase in cultured rat mesangial cells. *FEBS Lett* 370:141–145, 1995
6. Kawachi H, Orikasa M, Matsui K, *et al*: Epitope-specific induction of mesangial lesions with proteinuria by a MoAb against mesangial cell surface antigen. *Clin Exp Immunol* 88:399–404, 1992
7. Akagi Y, Isaka Y, Arai M, *et al*: Inhibition of TGF-beta1 expression by antisense oligonucleotides suppressed extracellular matrix accumulation in experimental glomerulonephritis. *Kidney Int* 50:148–155, 1996
8. Wanger R: Gene inhibition using antisense oligodeoxynucleotides. *Nature* 372:333–335, 1994

Kidney International, Vol. 66 (2004), pp. 2085–2087

EDITORIAL

Albumin turns on a vicious spiral of oxidative stress in renal proximal tubules

ENYU IMAI, HIDEAKI NAKAJIMA, and JUN-YA KAIMORI

Osaka and Tokyo, Japan, and Baltimore, Maryland

Albumin, the major component of proteinuria, is well recognized as a marker of renal diseases, particularly glomerular diseases. It is also known that the microalbuminuria, which reflects the endothelial disorder, predicts prognosis of the cardiovascular diseases. However, the albuminuria is not merely a sign of glomerular disease, but it causes proximal tubular cell injury.

Albumin uptake activates various signal transduction cascades in proximal tubule cells (Fig. 1). The activation of the intracellular signaling can be initiated by albumin endocytosis. In this process, activation of PI3 kinase may play important role in membrane traffic [1, 2]. It is less clear how the lysosome compartment holding albumin activates NADPH oxidase. However, activation of protein kinase C is implicated [3, 4]. Activated PKC, by which p47phox and p67phox, components of NAPDH oxidase, localized in cytosole as inactive forms, are translocated to membrane [5], activates NADPH oxidase and generates superoxide (O_2^-).

Akt-dependent p47phox activation in NADPH oxidase is also reported in leukocytes [6]. NADPH oxidase is abundantly localized in proximal convoluted tubule cells in kidney [7]. Superoxide is converted to hydrogen peroxide (H_2O_2) by SOD. H_2O_2 induces variety of intracellular signaling, such as MAP kinases (ERK1/ERK2, JNK, p38), PI3 kinase, AKT, JAK-STAT, AP-1, and NF-κB.

MAP kinase plays a critical role in determination of cell growth and death. H_2O_2 activates apoptosis signal-regulating kinase 1 (ASK1) by enhancing dimerization [8]. ASK1 promotes p38 and JNK phosphorylation. p38 activation, in particular, leads to apoptosis by activating caspases. Meanwhile, it is reported that H_2O_2 activates PI3K and Akt, which inhibits ASK1 activity in human embryonic kidney 293 cells [9]. Both signals are transduced in the cell in response to ROS; however, the net impact to determine the cell survival and death seems to depend on the strength of oxidative stress.

Key words: oxidative stress, glia maturation factor, angiotensin II, hydrogen peroxide, proximal tubule, proteinuria.

In protein overload model mouse, glia maturation factor-B (GMF-B) is induced in three weeks in proximal tubule cells, which may turn on the vicious cycle for ROS generation in proximal tubule [10]. GMF-B, a 17-kD intracellular protein, regulates the life/death signaling by activating p38 [11]. Kaimori et al [10] found that the overexpression of GMF-B causes augumented reorganization of F-actin, as well as vulnerability to oxidative stress, making cells more susceptible to apoptosis under oxidative stress. The reason for the susceptibility to cell death is that the H_2O_2 stimulation persists in GMF-B overexpressing cells, in which H_2O_2-generation enzyme, CuZn-SOD, is up-regulated, and the H_2O_2-reducing enzymes, glutathione peroxidase and catalase are down-regulated [10]. Recently, this phenomenon has been reconfirmed by astrocytes from GMF-B null mouse, which is resistant to death by H_2O_2 stimulation by decreasing CuZn-SOD [12].

Other major downstream signaling molecules from H_2O_2 stimulation are inflammation-related signaling molecules, such as NF-κB [3, 4] and JAK-STAT [13]. Numerous reports showed that albumin induced variety of effecter molecules through NF-κB, including MCP-1, RANTES, IL-8, PDGF, TGF-β, endothelin, and fractalkine [3, 4, 14]. IFN-γ–inducible genes, including interferon regulatory factor-1, MHC-I, MHC-II, and MCP-1 are up-regulated in albumin-overloaded proximal tubule without direct activation by IFN-γ [15]. Nakajima et al [13] revealed that the H_2O_2 generation by albumin uptake causes Jak2 activation and subsequent Stat1 and Stat5 phosphorylation in proximal tubular cells in culture. Overall, the net results of exposure of proximal tubule cells to albumin results in production of cocktail of cytokines and growth factors, which act in autocrine and paracrine manner.

In this issue of *Kidney International*, Wolf et al [16] have added new information to the complex albumin signaling cascade in proximal tubule. They demonstrated that the proximal tubule cells up-regulated TGF-β type II receptor by albumin. The promoter of the TGF-β type II receptor is regulated by AP1, which is induced by H_2O_2 stimulation. However, this induction was completely

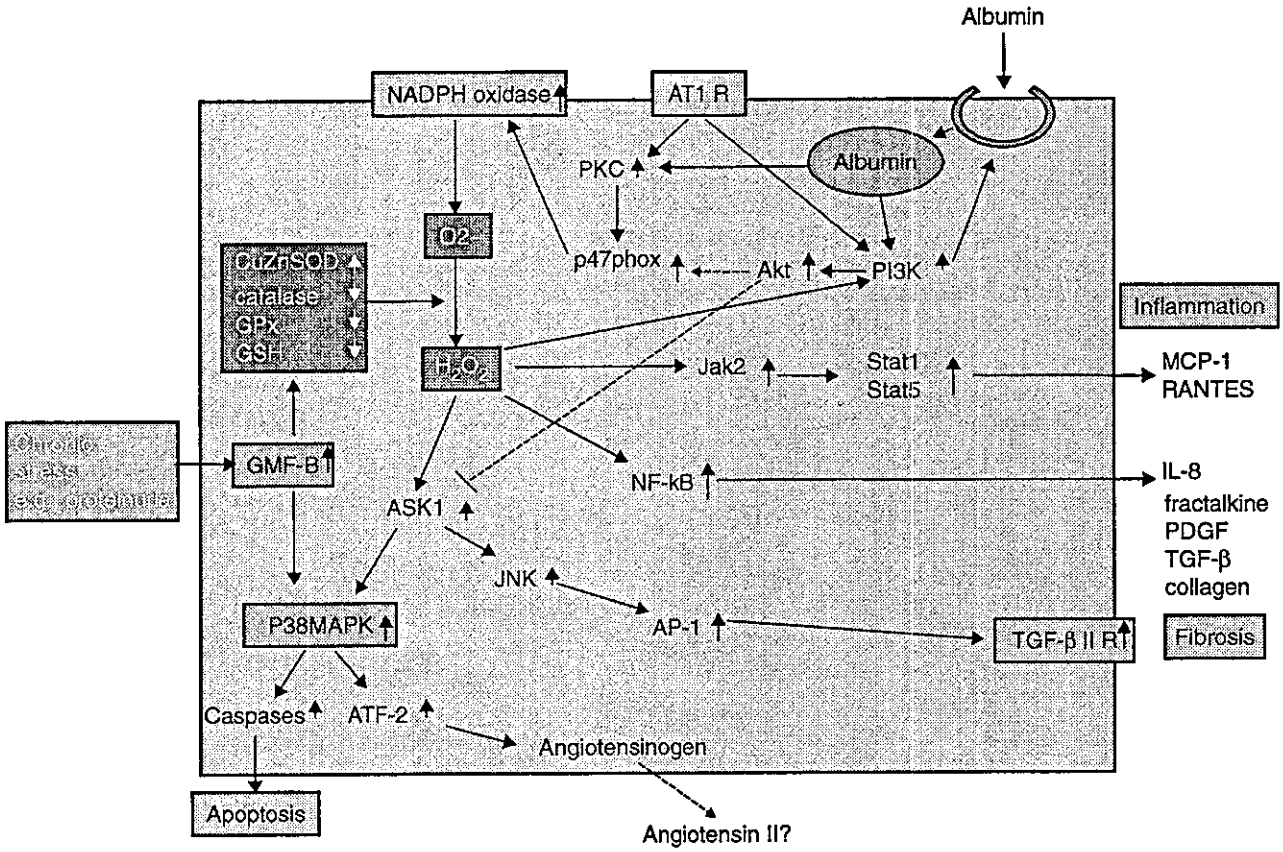

Fig. 1. Hypothetical signal transduction cascade of proximal tubule cells in response to protein overload. Arrows mean positive stimulation confirmed in tubular cells, and arrows with dot line means positive stimulation confirmed in another cells. Abbreviations: Akt, protein kinase B; AP-1, activator protein-1; ASK-1, apoptosis signal-regulating kinase-1; AT1 R, angiotensin type 1 receptor; ATF-2, activating transcription factor-2; CuZnSOD, cupper zinc superoxide dismutase; GMF-B, glia maturation factor; GPx, glutathione peroxidase; GSH, glutathione; Jak, Janus protein kinase; JNK, c-JUN N-terminal kinase; MCP-1, macrophage chemoattractant protein-1; NF-κB, nuclear factor κB; p47phox, 47 kD subunit of the phagocyte oxidase; PDGF, platelet-derived growth factor; PI3K, phosphatidylinositol 3-kinase; PKC, protein kinase C; PKC, protein kinase C; RANTES, regulated on activation, normally T cell–expressed and –secreted; Stat, signal transducers and activators of transcription; TGF-β, transforming growth factor-β; TGF-β II R, transforming growth factor-β type II receptor.

abolished by angiotensin II (Ang II) type 1 receptor antagonist, suggesting Ang II–mediated TGF-β type II receptor induction. They speculated that albumin leads to tubular synthesis of Ang II, although they did not show the activation of local Ang II generation in proximal tubule cells. How can we reconcile the new finding of involvement of Ang II in proximal tubule activation by albumin? Hsieh et al [17] reported that ROS induced angiotensinogen in proximal tubule cells exposed to high glucose. They showed that p38 is involved the angiotensinogen gene up-regulation by ROS stimulation. They speculated that the phosphorylation of the nuclear activating transcription factor-2 (TFA-2) via p38 may activate the angiotensinogen gene transcription by binding of ATF-2 and CREB heterodimer to the cAMP-responsive element of the promoter. These results imply the potential that another vicious cycle can be turned on by activation of local Ang II generation by albumin overload.

How can we clinically apply the identification of the signaling effects of albumin in proximal tubule? The complex signal cascade provides the possibility of the multiple means of intervention and modulation against inflammation, fibrosis, and apoptosis.

Given that local Ang II generation is enhanced and, consequently, oxidative stress is exaggerated, AT1 antagonist, which also hemodynamically reduces proteinuria, can cut off the vicious cycle for ROS generation due to autocrine Ang II generation in tubular cells. Moreover, some angiotensin receptor antagonists may directly reduce the oxidative injury by antioxidative action of lowering the formation of carbon-central radicals and hydroxyl-radicals [18]. In contrast, the mechanism of the other vicious cycle generated by GMF-B activation is largely unknown. Potential involvement of protein kinase A in the activation of GMF-B was shown in C6 cells [11]; however, no report has been published concerning

the mechanism of GMF-B induction except for albumin overload in proximal tubule. The elucidation of GMF-B activation in proximal tubule may provide a new avenue of the therapy for chronic proteinuric nephropathy.

Correspondence to Enyu Imai, Department of Internal Medicine and Therapeutics, Osaka University Graduate School of Medicine, Osaka, Japan.
E-mail: imai@medone.med.osaka-u.ac.jp

REFERENCES

1. Roth M: Phosphoionsitides in constitutive membrane traffic. *Physiol Rev* 84:699–730, 2004
2. Brunskill N, Tobin A, Nahorski S, Walls J: Receptor-mediated endocytosis of albumin by kidney proximal tubule cells is regulated by phophatidylinositide 3-kinase. *J Clin Invest* 101:2140–2150, 1998
3. Tang S, Leung J, Abe K, *et al*: Albumin stimulates interleukin-8 expression in proximal tubular epithelial cells in vitro and in vivo. *J Clin Invest* 111:515–527, 2003
4. Morigi M, Macconi D, Zoja C, *et al*: Protein overload-induced NF-κB activation in proximal tubular cells requires H_2O_2 through a PKC-dependent pathway. *J Am Soc Nephrol* 13:1179–1189, 2002
5. Babior B: NADPH: An update. *Blood* 93:1464–1476, 1999
6. Hoyal C, Gutierrez A, Young B, *et al*: Modulation of p47PHOX activity by site-specific phosphorylation: Akt-dependent activation of the NADPH oxidase. *Proc Natl Acad Sci USA* 100:5130–5135, 2003
7. Geiszt M, Kopp J, Varnai P, Leto T: Identification of renox, an NAD(P)H oxidase in kidney. *Proc Natl Acad Sci USA* 97:8010–8014, 2000
8. Gotoh Y, Cooper J: Reactive oxygen species- and dimerization-induced activation of apoptosis signal-regulating kinase 1 in tumor necrosis factor-alpha signal transduction. *J Biol Chem* 273:17477–17482, 1998
9. Kim A, Khursigara G, Sun X, *et al*: Akt phosphorylates and negatively regulates apoptosis signal-regulating kinase 1. *Mol Cell Biol* 21:893–901, 2001
10. Kaimori J, Takenaka M, Nakajima H, *et al*: Induction of glia maturation factor-beta in proximal tubular cells leads to vulnerability to oxidative injury through the p38 pathway and changes in antioxidant enzyme activities. *J Biol Chem* 278:33519–33527, 2003
11. Lim R, Zaheer A: In vitro enhancement of p38 mitogen-activated protein kinase activity by phosphorylated glia maturation factor. *J Biol Chem* 271:22953–22956, 1996
12. Zaheer A, Yang B, Cao X, Lim R: Deacresed copper-zinc superoxide activity and increased resistance to oxidative stress in glia maturation factor-null astrocytes. *Neurochem Res* 29:1437–1480, 2004
13. Nakajima H, Takenaka M, Kaimori J, *et al*: Activation of the signal transducer and activator of transcription signaling pathway in renal proximal tubular cells by albumin. *J Am Soc Nephrol* 15:276–285, 2004
14. Donadelli R, Zanchi C, Morigi M, *et al*: Protein overload induces fractalkine upregulation in proximal tubular cells through nuclear factor kappaB- and p38 mitogen-activated protein kinase-dependent pathways. *J Am Soc Nephrol* 14:2436–2446, 2003
15. Nakajima H, Takenaka M, Kaimori J, *et al*: Gene expression profile of renal proximal tubules regulated by proteinuria. *Kidney Int* 61:1577–1587, 2002
16. Wolf G, Schroeder R, Ziyadeh F, Stahl RAK: Albumin upregulates the type II transforming growth factor-beta receptor in cultured proximal tubular cells. *Kidney Int* 66:1849–1858, 2004
17. Hsieh T, Zhang S, Filep J, *et al*: High glucose stimulates angiotensinogen gene expression via reactive oxygen species generation in rat kidney proximal tubular cells. *Endocrinology* 143:2975–2985, 2002
18. Miyata T, Strihou C, Ueda Y, *et al*: Angiotensin II receptor antagonist and angiotensin converting enzyme inhibitors lower in vitro the formatio of advanced glycogen end products: Biochemical mechanisms. *J Am Soc Nephrol* 13:2478–2487, 2002

Extracellular Matrix Glycoprotein Biglycan Enhances Vascular Smooth Muscle Cell Proliferation and Migration

Ryoko Shimizu-Hirota, Hiroyuki Sasamura, Mari Kuroda, Emi Kobayashi, Matsuhiko Hayashi, Takao Saruta

Abstract—Proteoglycans are produced and secreted by vascular smooth muscle cells, but the pathophysiological role of these glycoproteins in the vasculature is an enigma. Because the small leucine-rich proteoglycan (SLRP) biglycan is overexpressed in arteriosclerotic lesions, we produced mice constitutively overexpressing biglycan in the vascular smooth muscle, in order to examine the effects on vascular pathology. In the aorta and renal vasculature, increased vascular proliferation was seen both in the basal state and after infusion of angiotensin II (Ang II) in the transgenic mice compared with wild-type controls. In addition, the combination of biglycan overexpression and Ang II infusion resulted in marked increases in vascular smooth muscle cell proliferation and migration in the coronary arteries, as well as increases in fibrosis surrounding the vessels. In vitro, biglycan caused an increase in thymidine incorporation and migration of vascular smooth muscle cells, whereas these parameters were unchanged or reduced in endothelial cells. Moreover, addition of biglycan resulted in an increase in cdk2 expression and decrease in p27 levels in the vascular smooth muscle cells. These results suggest that this extracellular matrix SLRP may be involved in the regulation of vascular smooth muscle growth and migration through cdk2- and p27-dependent pathways. Furthermore, changes in biglycan expression could be a factor influencing the susceptibility of arteries to vascular injury, and may play a direct role in the pathogenesis of vascular lesions. (*Circ Res.* 2004;94:1067-1074.)

Key Words: proteoglycan ■ vascular injury ■ angiotensin

The cells in the vascular wall are held together by a complex network of macromolecules that collectively form the extracellular matrix. The species of glycoproteins known as proteoglycans are an important component of this matrix. These glycoproteins consist of a core protein covalently bound to one or more glycosaminoglycan (GAG) side chains.[1] Based on the composition of the GAG moiety, the proteoglycans may be classified into chondroitin sulfate, dermatan sulfate, heparan sulfate, and keratan sulfate proteoglycans. In the vascular wall, a major proteoglycan synthesized by endothelial cells and vascular smooth muscle cells is the proteoglycan biglycan, which consists of a core protein bound to two chondroitin sulfate/dermatan sulfate side chains.

Biglycan is a member of the small leucine-rich proteoglycan (SLRP) family of proteoglycans, which are characterized by the presence of repeated sequences containing a high proportion of leucine residues.[2] Recent studies have suggested that these SLRPs are not simply an inert structural component of the extracellular matrix, but may be actively involved in the control of collagen deposition, and the activation and inactivation of cytokines and growth factors.[1,3]

Studies from our and other laboratories have shown that biglycan expression is markedly altered in disease states, and that therapeutic intervention with hormones or antihypertensive agents can alter biglycan expression in vivo and in vitro.[4–6] Of importance, biglycan expression in the blood vessel wall has been shown to be increased in atherosclerotic lesions and restenotic lesions both in animal models[7,8] and in human samples.[9,10]

At present, the functions of biglycan in the blood vessel wall are still unclear. In this study, we used a vascular smooth muscle cell–specific promoter to amplify biglycan expression in the vasculature, and examined the susceptibility of these vessels to vascular injury mediated by angiotensin II infusion. We also examined if biglycan can affect growth and migratory properties in vascular smooth muscle cells in vitro.

Materials and Methods

Production of Transgenic Mice Overexpressing Biglycan in the Vasculature

A transgenic construct was produced by ligating the human smooth muscle α-actin promoter[11] (pBS-HSMA-EA4.7, generously provided by Dr Miwa, Osaka University, Osaka, Japan) upstream of the human biglycan cDNA[2] (P16, generously provided by Dr Fisher, National Institute of Dental and Craniofacial Research, Bethesda, Md). Purified DNA was microinjected into fertilized ova of C56BL/6J mice using standard techniques. Transgenic mice were identified by PCR and Southern blotting, and further experiments

Original received August 20, 2003; resubmission received February 6, 2004; revised resubmission received March 5, 2004; accepted March 9, 2004.
From the Department of Internal Medicine, School of Medicine, Keio University, Tokyo, Japan.
Correspondence to Hiroyuki Sasamura, Department of Internal Medicine, School of Medicine, Keio University, 35 Shinanomachi, Shinjuku-ku, Tokyo 160-8582, Japan. E-mail sasamura@sc.itc.keio.ac.jp

Circulation Research is available at http://www.circresaha.org DOI: 10.1161/01.RES.0000126049.79800.CA

were performed on two independent transgenic lines. All animal experiments were performed in accordance with institutional guidelines.

Analysis of Transgene Expression by RT-PCR-RFLP and Immunohistochemistry

Total RNA was purified from aorta, kidney, heart, lung, testis, and skeletal muscle by the acid guanidine-phenol-chloroform method, and quantified by absorbance at 260 nm in a spectrophotometer. Semiquantitative RT-PCR was performed using protocols described by us previously.[5,6] The biglycan primers used corresponded to an area of complete homology in the nucleotide sequences of human and mouse biglycan cDNA and spanned several introns in the genomic sequence. Moreover, the amplified cDNA products could be distinguished by the digestion with the restriction enzyme *SacI* because the human cDNA contains an internal *SacI* site, resulting in two DNA fragments (228 bp and 177 bp) after digestion of amplified DNA derived from transgenic transcription products, whereas the native biglycan transcript yielded one fragment of size 405 bp. Thus, comparison of the abundance of the DNA of these sizes allows an estimate of the relative levels of mRNA expression derived from the native biglycan gene and transgenic biglycan cDNA, respectively. RT-PCR of transforming growth factor-β_1 (TGF-β_1) and glyceraldehyde-3-phosphate dehydrogenase (GAPDH) mRNA was performed as described.[5,12]

Immunohistochemistry of biglycan expression in the aorta was performed using an anti-human biglycan antibody (LF-51)[2] kindly provided by Dr Fisher (National Institute of Dental and Craniofacial Research, Bethesda, Md). Deparaffinized samples were pretreated with chondroitinase ABC for 1 hour, then subjected to immunohistochemistry as described later.

Animal Treatments and Assays

Eight-week-old male heterozygous transgenic mice were infused with Ang II (1 μg/kg/min) or vehicle (saline) for 2 weeks using osmotic minipumps (Alzet). Wild-type littermates were used as controls. Blood pressures were measured by tail-cuff plethysmography. Mice were euthanized by ether anesthesia and tissue samples of aorta, heart, and kidneys were fixed by rapid immersion in 4% paraformaldehyde (PFA), before embedding in paraffin. Preliminary experiments were performed to compare the results seen in mice perfusion-fixed at blood pressure before euthanasia versus mice that had not been perfusion-fixed. These experiments confirmed that similar differences between the groups were obtained with or without perfusion-fixation at blood pressure. Aortic sections were stained with Azan, whereas heart and kidney sections were stained with the Masson trichrome stain. Plasma renin activity was measured by standard techniques.[5]

Measurement of Collagen Content

Cardiac collagen content was assessed by estimation of hydroxyproline content. Cardiac sections were hydrolyzed by treatment with 6 mol/L HCl at 115°C for 24 hours, then hydroxyproline content in the lyophilizes samples was estimated by reaction with chloramine T and p-dimethylaminobenzaldehyde.[13]

Morphometric and Immunohistochemical Analyses

Media thickness and lumen diameters in the vasculature were measured using NIH image computer software. The lumen diameter was calculated from the lumen circumference, assuming that the vessel is circular, and the media/lumen ratio calculated by dividing the media thickness by the lumen diameter. For the assessment of perivascular fibrosis, the area of fibrosis (collagen deposition stained with aniline blue) immediately surrounding the coronary arterial wall was measured, and the fibrotic index was determined as the area of fibrosis divided by total vessel area. To estimate the incidence of coronary stenosis/occlusion, the three main coronary arteries were examined, and the heart was defined to have a coronary stenotic lesion if at least one neointimal lesion occupying >30% of the lumen area was seen. Immunohistochemical analyses were performed on PFA-fixed paraffin-embedded 5-um sections by the streptavidin-biotin-peroxidase method. Briefly, after deparaffination and quenching of endogenous peroxidase with 0.3% hydrogen peroxidase in methanol for 30 minutes, serial sections were incubated with 2% normal goat serum to reduce nonspecific background staining, then incubated with polyclonal antibodies directed against proliferating cell nuclear antigen (PCNA), α-smooth muscle actin, CD68, or CD31 at a dilution of 1:100. Negative control experiments were performed by replacing the primary antibodies with normal rabbit serum. Subsequently, biotinylated secondary antibody and then streptavidin conjugate were applied. Positive staining was visualized with either DAB or tetra-methyl-benzidine using a commercially available kit (Toyobo).

In Vitro Studies

In vitro studies were performed on rat VSMCs[4] and bovine aortic endothelial cells. Assessment of cell proliferation, collagen synthesis, cell migration, and Western blot analysis of cell cycle proteins was performed based on previously described protocols,[14,15] which are presented in the expanded Materials and Methods section of the online data supplement (available at http://circres.ahajournals.org).

Statistical Analyses

Results are expressed as the mean±SEM. Statistical comparisons were made by ANOVA followed by Fisher's post hoc test. Growth curves were compared using repeated measures ANOVA. Values of $P<0.05$ were considered statistically significant.

Results

Expression of Human Biglycan in Biglycan Transgenic Mice

The transgene construct contained the mouse α-smooth muscle actin promoter ligated to the coding sequence of human biglycan cDNA. This promoter effects a pattern of transgene expression similar to that of the endogenous α-smooth muscle actin, which is the dominant actin isoform in vascular tissue. Six founder mice containing the human biglycan transgene were identified by PCR and Southern blot analysis, and two lines were propagated and used for subsequent experiments. Figure 1 shows the results of a representative experiment to examine the expression of biglycan in the aorta of transgenic mice and their nontransgenic littermates. The presence of the biglycan transgene DNA in tail genomic DNA was assessed using PCR primers spanning intron 2, which yielded a 263-bp PCR product in the case of the intronless transgene, and 550-bp PCR product in the case of the native biglycan gene. Expression of biglycan mRNA in the aorta was assessed by RT-PCR. We have shown that RT-PCR performed in the linear phase of the amplification reaction enables a comparison of total biglycan mRNA expression between different animals.[5] Moreover, because the primers correspond to identical sequences of the human and mouse biglycan cDNA sequences, and only human biglycan cDNA sequence contains a *SacI* site, relative levels of transgene and native biglycan mRNA expression in the same animal could also be directly assessed by comparison of the amplified bands after the addition of a *SacI* digestion step after RT-PCR. These methods suggested that biglycan mRNA was increased (≈2- to 4-fold) in the transgenic mice aorta. In contrast, biglycan mRNA from the transgene was below detectable levels in other tissues such as kidney, heart, lung, testis, and skeletal muscle (Figure 1C). To further confirm overexpression of human biglycan in the vasculature,

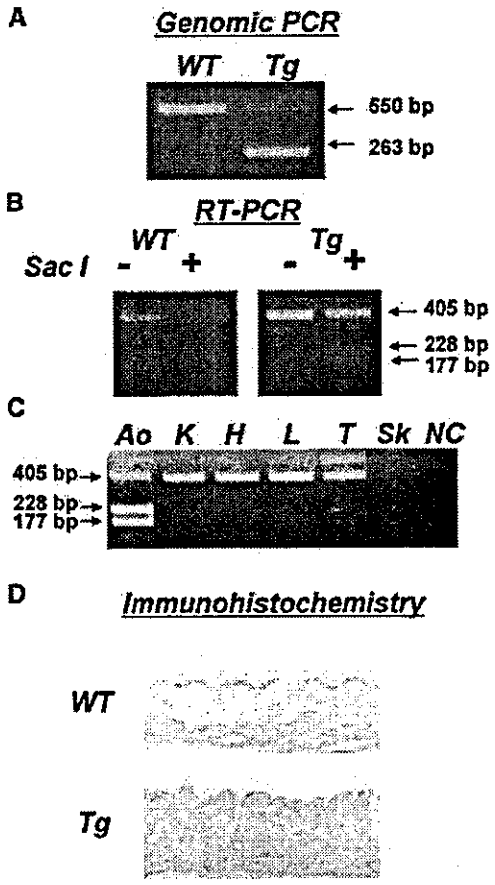

Figure 1. Characterization of mice with vascular smooth muscle–specific overexpression of biglycan. A, Representative result of PCR of tail DNA. Transgene yields a 263-bp PCR product, whereas the native biglycan gene yields a 550-bp PCR product. B, Representative result of *Sac*I digestion of RT-PCR product from aorta mRNA. RT-PCR product derived from the transgene mRNA yields 2 fragments (228 and 177 bp) after *Sac*I digestion. C, RT-PCR analysis of native and transgenic biglycan mRNA in aorta (Ao), kidney (K), heart (H), lung (L), testis (T), and skeletal muscle (Sk) of transgenic mice. All samples were digested with *Sac*I before electrophoresis to yield 2 fragments (228 and 177 bp) in the case of biglycan mRNA derived from the transgene, whereas the native biglycan mRNA is undigested (405 bp). NC indicates negative control. D, Immunohistochemical staining of wild-type (WT) and transgenic (Tg) mouse aorta using an anti-human biglycan antibody (LF-51).

immunohistochemical staining was performed. Positive staining for biglycan protein was substantially increased in the medial layer of biglycan-transgenic mice compared with their wild-type littermates (Figure 1D).

Effects of Biglycan Overexpression on the Aorta, Coronary Arteries, and Renal Arterioles

The effects of biglycan overexpression on the structure of large (aorta), medium-sized (coronary arteries), and small (renal arterioles) arteries were examined. Preliminary experiments suggested that proliferating cells in the vascular media stained by PCNA were increased compared with controls, resulting in increased medial thickness. To confirm these findings, mice were divided into 4 groups: groups 1 and 2 were wild-type mice, and groups 3 and 4 were transgenic mice. Groups 1 and 3 were treated with vehicle, whereas groups 2 and 4 were infused with a pressor dose of Ang II to accentuate vascular hypertrophy and hyperplasia. Online Table 1 (available in the online data supplement at http://circres.ahajournals.org) shows the results of changes in heart and body weight, blood pressure, and plasma renin activity in the groups with and without Ang II infusion. The initial body and heart weights were similar in the transgenic mice and wild-type mice, and the heart/body weight ratios were significantly increased after Ang II infusion in groups 2 and 4. Baseline systolic blood pressure did not differ significantly between the 4 groups. Ang II increased systolic blood pressure from 100±3 to 132±7 mm Hg in wild-type mice (group 2) and from 103±4 to 136±2 mm Hg in transgenic mice (group 4). We also measured PRA from blood samples of the 4 groups at the end of the study. PRA was below the detection level in the Ang II–treated groups (2 and 4). No significant change in PRA was found between the untreated wild-type and transgenic mice. The changes in native and transgenic biglycan mRNA in the Ang II–treated and –untreated groups are shown in Figure 2A. Consistent with our previous report,[4] Ang II treatment resulted in an increase in the native biglycan, but did not cause a significant change in the transgenic biglycan mRNA. Aortic and cardiac TGF-β1 mRNA was also increased by Ang II treatment, but no major differences were observed between wild-type and transgenic mice (Figures 2B and 2C).

Morphological changes in the aorta, coronary arteries, and renal arterioles were assessed. As shown in Figure 3, an increase in PCNA-positive cell counts was seen in the aorta of the transgenic mice compared with wild-type littermates. Moreover, increased media/lumen ratios were also seen in these vessels. Similar results were seen in the renal arterioles (Figure 4). In the case of the coronary arteries, more pronounced changes were seen (Figures 5 and 6). In the Masson-trichrome–stained sections, the effect of Ang II to cause cellular proliferation was accentuated in the biglycan transgenic mice, resulting in a dramatic proliferation of cells with areas of partial stenosis/occlusion of the coronary arteries in mice of group 4 (transgenic mice treated with Ang II) (Figure 5A). The incidence of coronary artery stenosis (defined as the presence of at least one lesion occupying >30% of the lumen) in the four groups of mice were as follows: wild-type Ang II (−) 0/15 (0%); wild-type Ang II (+) 2/15 (13%); transgenic Ang II (−) 0/18 (0%); and transgenic Ang II (+) 16/26 (62%).

The prominent lesions seen in the transgenic mice treated with Ang II were examined immunohistochemically. Quantitation of PCNA-positive cell counts revealed significant elevation in the transgenic mice with or without Ang II infusion compared with wild-type mice (Figure 5B). To characterize the cell types responsible for the stenotic lesions, staining was also performed using specific markers. It was found that the intimal cells stained strongly for α-smooth muscle cell actin, suggesting that the cells were derived from proliferating vascular smooth muscle cells (Figure 6).

We also assessed perivascular fibrosis in the coronary arteries by measurement of the fibrotic index. Both untreated

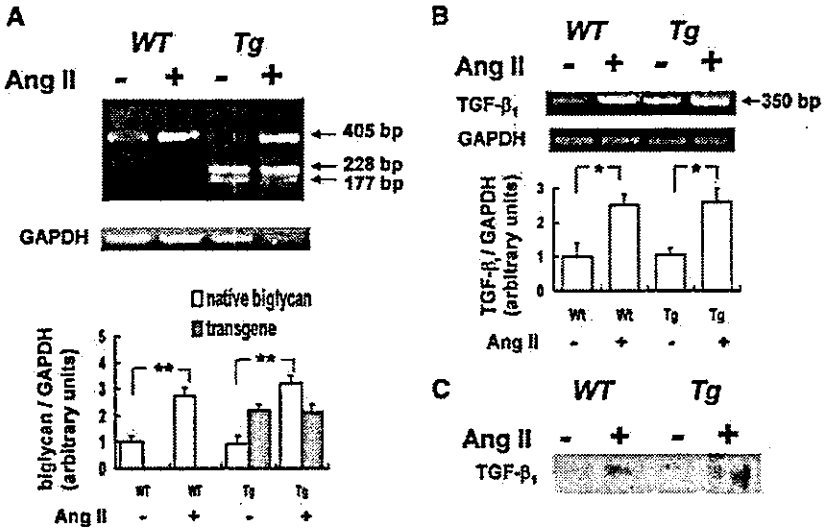

Figure 2. A, RT-PCR-RFLP analysis of biglycan mRNA from the aorta of wild-type (WT) and transgenic (Tg) mice with and without Ang II treatment. All samples were digested with *Sac*I before electrophoresis to yield 2 fragments (228 and 177 bp) in the case of biglycan mRNA derived from the transgene, whereas the native biglycan mRNA is undigested (405 bp). Top, Representative result of RT-PCR analysis. Bottom, Results of densitometric analysis; $^{**}P<0.01$ (n=5 per group). B, RT-PCR analysis of TGF-β_1 mRNA from the aorta of wild-type (WT) and transgenic (Tg) mice with and without Ang II treatment; $^{*}P<0.05$ (n=5 per group). C, Western blot analysis of TGF-β_1 in the hearts of wild-type (WT) and transgenic (Tg) mice with and without Ang II treatment.

and Ang II–treated transgenic mice showed increased fibrotic index compared with the wild-type mice (Figure 5C). Assessment of cardiac collagen content was also performed by measuring hydroxyproline content in cardiac sections. Although baseline cardiac collagen content did not differ significantly between the transgenic and the wild-type mice, Ang II treatment resulted in a greater increase (1.7-fold change from 1.13±0.14 to 1.90±0.20 μmol/g; $P<0.05$) in the transgenic mice compared with wild-type mice (1.2-fold change from 1.30±0.29 to 1.55±0.28 μmol/g; P=NS).

Effects of Biglycan on VSMC Proliferation, Collagen Synthesis, and Migration In Vitro

To further examine the effects of biglycan on the vasculature, experiments were performed on cultured vascular cells (VSMCs and endothelial cells) in vitro. Figure 7 shows the effects of biglycan on VSMC growth. Biglycan caused an increase in VSMC numbers, and a dose-dependent increase in thymidine incorporation by VSMCs, whereas an opposite trend was found in thymidine incorporation in the case of endothelial cells. The effects of biglycan were additive with the effects of Ang II. Biglycan also caused a significant increase in collagenase-sensitive proline incorporation in Ang II–treated VSMCs but not in endothelial cells.

We next examined the migratory response to biglycan in VSMC and endothelial cells. As shown in Figure 7, biglycan treatment elicited a robust migratory response in VSMCs, and further enhanced the Ang II–induced migratory response. In contrast, no apparent change was seen in endothelial cell migration.

Western Blot Analysis of Intracellular Signaling Pathways of Biglycan in Vascular Cells

The effects of biglycan on the expression of genes affecting VSMC proliferation were examined by Western blot analysis. As shown in Figure 8, stimulation with biglycan resulted in an enhancement of cdk2 expression within 6 hours in VSMCs. In contrast, levels of p27 were reduced at 24 hours, whereas p21 expression remained at low levels throughout the experiment.

Discussion

Biglycan is a major glycoprotein of the extracellular matrix.[1–3] Biochemically, it belongs to the SLRP family of proteoglycans and is composed of a distinct core protein covalently bound to two chondroitin sulfate/dermatan sulfate-containing glycosaminoglycan side chains.

The functions of biglycan are only beginning to be understood. Similar to decorin, biglycan has been shown to bind TGF-β in vitro[16]; however, there is controversy whether biglycan exerts TGF-β inhibitory effects in vivo.[17] Biglycan has also been shown to associate with type I[18] and type VI[19] collagens in vitro, suggesting a role in the control of collagen fibrillogenesis. Indeed, targeted disruption of the biglycan gene results in a phenotype characterized by abnormal collagen fibrils in tendons, together with abnormal bone structure and reduced bone mass.[20,21]

Biglycan is known to be expressed in the arterial wall and has been purified from the normal human aorta.[22] However, the role of biglycan in the vasculature is unclear. Of note is the fact that expression of biglycan is markedly upregulated in diseased arteries, including atherosclerotic lesions,[9] arteriolosclerotic lesions,[23] areas of restenosis postangioplasty,[10] and in transplant coronary arteriopathy.[24] Of interest, it has been reported that biglycan colocalizes with apolipoprotein E in atherosclerotic plaques,[9] suggesting the hypothesis that biglycan, by virtue of its ability to bind apolipoproteins, may be directly involved in the retention of these atherogenic molecules in the diseased vessel wall.

Because the upregulation of biglycan in diseased arteries suggested a role in vascular disease, our aim in this study was to examine the direct consequences of increasing biglycan content in the vessel wall. To this end, transgenic mice that overexpressed biglycan in the vasculature were produced using a transgene construct consisting of the human biglycan cDNA ligated downstream of the smooth muscle cell α-actin promoter. Experiments were performed on two transgenic lines that yielded similar results.

No gross changes in the development or behavior of the transgenic mice were observed compared with their nontrans-

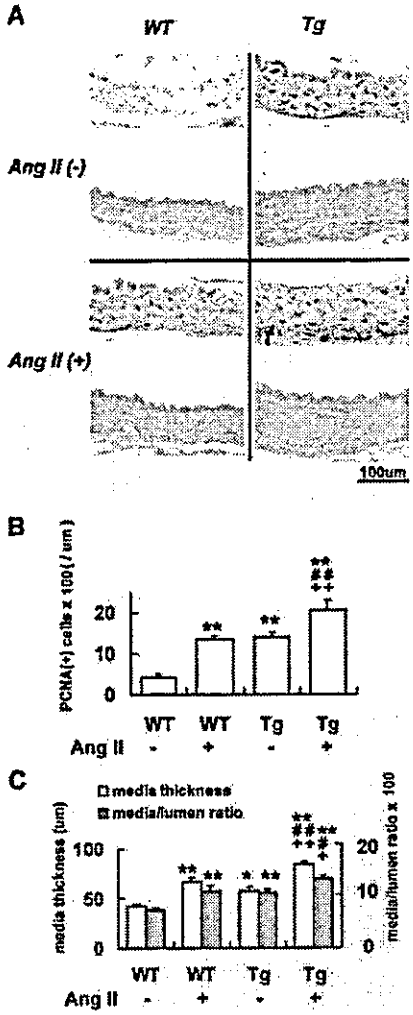

Figure 3. Vascular morphology of aorta of wild-type (WT) and transgenic (Tg) mice with and without Ang II treatment. A, Representative cross sections of aortic wall. Top photomicrograph, PCNA immunostaining; bottom photomicrograph, Azan stain. Original magnification ×100. B, Quantitation of PCNA-positive cell counts in aorta of wild-type and transgenic mice. C, Quantitation of media thickness and media/lumen ratios in aorta of wild-type and transgenic mice.*$P<0.05$, **$P<0.01$ vs wild-type [Ang II (−)]; +$P<0.05$, ++$P<0.01$ vs Tg [Ang II (−)]: #$P<0.05$, ##$P<0.01$ vs wild-type [Ang II (+)] (n=8 to 16 per group).

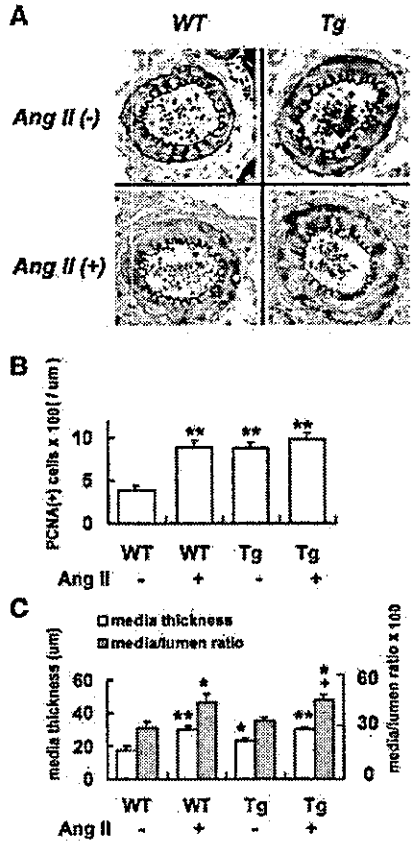

Figure 4. Vascular morphology of renal arterioles of wild-type (WT) and transgenic (Tg) mice with and without Ang II treatment. A, Representative Azan stain of renal arteriole wall. B, Quantitation of PCNA-positive cell counts in renal arterioles of wild-type and transgenic mice. C, Quantitation of media thickness and media/lumen ratios in renal arteriole of wild-type and transgenic mice. *$P<0.05$, **$P<0.01$ vs wild-type [Ang II (−)]; +$P<0.05$ vs Tg [Ang II (−)] (n=8 to 16 per group).

genic littermates. Moreover cardiac echocardiography did not reveal a major difference in ejection fraction between untreated transgenic and wild-type mice (data not shown). However, increased proliferation of the aortic wall and renal arterioles was seen, which was evidenced by increased numbers of PCNA-positive cells in these vessels, accompanied by increases in the medial thickness of the vessels.

In this study, we examined the effects of infusion of Ang II on the vasculature in wild-type and transgenic mice, because Ang II is a peptide hormone that is thought to play a major role in the progression of vascular disease, a concept which has been underscored by the efficacy of Ang receptor blockade in attenuating the progression of hypertensive vascular disease. Ang II infusion resulted in an increase in vascular hypertrophy and proliferation of vascular cells, and these effects were enhanced in the aorta of the transgenic the mice. Another notable finding were the lesions seen in the coronary arteries of the Ang II–infused transgenic mice, which were reminiscent of vascular lesions in coronary disease, with marked increases in the vascular intima, resulting in some cases in partial occlusion of coronary arteries, together with increases in perivascular fibrosis.

Concerning the mechanisms of these changes, we found that stimulation of VSMCs with biglycan resulted in an increase in thymidine incorporation, an effect that was additive with Ang II. These results were consistent with the in vivo findings in the transgenic mice and provided further evidence that biglycan has a proliferative effect on VSMCs.

It is well known that VSMC proliferation is coordinately regulated by cell cycle proteins. Activation of a cdk2-cyclin complex during the G1 phase is involved in the G1 to S phase transition, and this complex is inhibited by the cdk inhibitor p27.[25] Therefore, our findings that biglycan enhances cdk2 kinase expression while diminishing p27 levels is consistent with the proliferative effects of biglycan that we found both in vivo and in vitro. It has been suggested that cell cycle

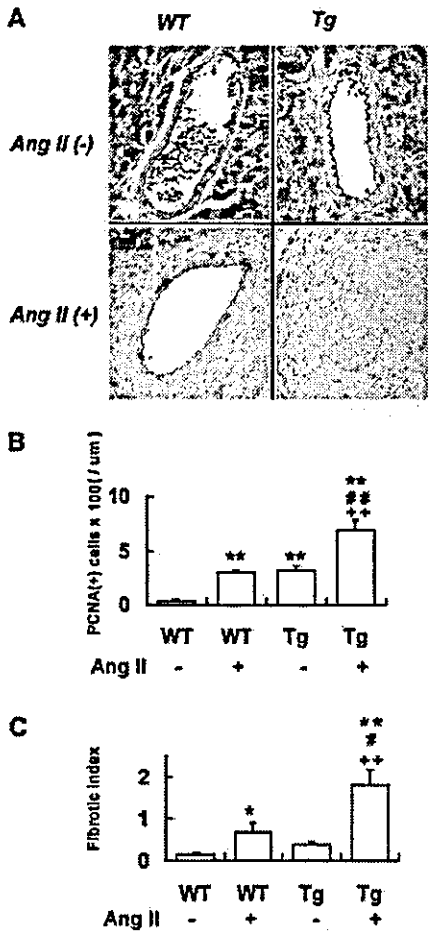

Figure 5. Vascular and perivascular morphology of coronary arteries of wild-type (WT) and transgenic (Tg) mice with and without Ang II treatment. A, Representative micrographs of coronary artery sections stained with Masson-trichrome in wild-type and transgenic mice. Original magnification ×200. B, Quantitation of PCNA-positive cell counts in coronary arteries of wild-type and transgenic mice. C, Quantitation of perivascular fibrosis in coronary arteries of wild-type and transgenic mice. *$P<0.05$, **$P<0.01$ vs wild-type [Ang II (−)]; ++$P<0.01$ vs Tg [Ang II (−)]: #$P<0.05$, ##$P<0.01$ vs Wild-type [Ang II (+)] (n=8 to 16 per group).

proteins may also regulate VSMC migration.[26] Taken together, our results suggest that the observed phenotype in the biglycan transgenic mice could be explained by the effects on these intracellular proteins.

It should be noted that the proliferative effects of biglycan appeared to depend on the cell type, because biglycan caused a decrease in thymidine incorporation in cultured endothelial cells in clear contrast to the effects on VSMCs. Similarly, biglycan increased migration in VSMCs but not in endothelial cells. With regards to the effects of biglycan on other cells, biglycan has been suggested to stimulate growth and differentiation of monocytic lineage cells and brain microglial cells, whereas in pancreatic cancer cells proliferation was suppressed by biglycan, and in mesangial cells biglycan had no significant effect alone, but inhibited the proliferative effects of PDGF-BB.[27–29] Of further interest is the fact that

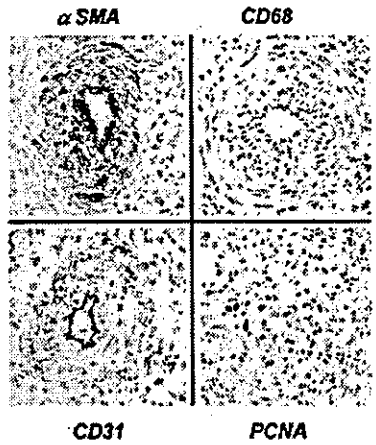

Figure 6. Immunohistochemical assessment of coronary lesions in Ang II–treated transgenic mice. A, Results of immunostaining of coronary arteries from Ang II–infused transgenic mice with antibodies to α-smooth muscle cell actin (αSMA), CD68 (marker for macrophages), CD31 (marker for endothelial cells), and PCNA. Original magnification ×200.

the related SLRP decorin has been shown to induce p21, p27, and growth arrest in many cell types including both VSMCs and endothelial cells.[30,31] Taken together, these results suggest that biglycan and decorin found in the extracellular matrix may be involved in the cell-specific regulation of cell proliferation and growth. It remains to be determined whether the differences between biglycan and decorin exist because of differences in the core protein structure, or the number of glycosaminoglycan side-chains associated with these two related molecules.

In the in vivo experiments using biglycan transgenic mice, we did not differentiate between the influence of Ang II per se on the vasculature, versus the indirect effects of the increased blood pressure mediated by Ang II. Because comparable results were seen in cultured VSMCs in vitro, it is probable that the effects on cell growth and perivascular fibrosis in vivo may be attributed at least in part to biglycan modulating a direct (blood pressure–independent) effect of Ang II on the vasculature in the transgenic mice. However, the possibility that a blood pressure–mediated mechanism could also contribute to the changes cannot be ruled out. Another possibility is that changes in growth factor expression could be involved as an intermediary mechanism. The fact that major differences in TGF-β1 mRNA were not found between the wild-type and transgenic mice suggest that changes in the expression of this growth factor do not play a major role in the observed changes.

The results of this study have several implications for the understanding of vascular biology and the pathogenesis of vascular injury. In designing the study, our initial hypothesis was that biglycan overexpression would result in an attenuation of vascular injury, because the related SLRP decorin is a potential candidate for the gene therapy of diseases such as postangioplasty restenosis, pulmonary fibrosis, and renal glomerulosclerosis.[32–34] In fact, the results of this study suggest that the upregulation of biglycan reported in diseased arteries may contribute directly to the pathogenesis of vascu-

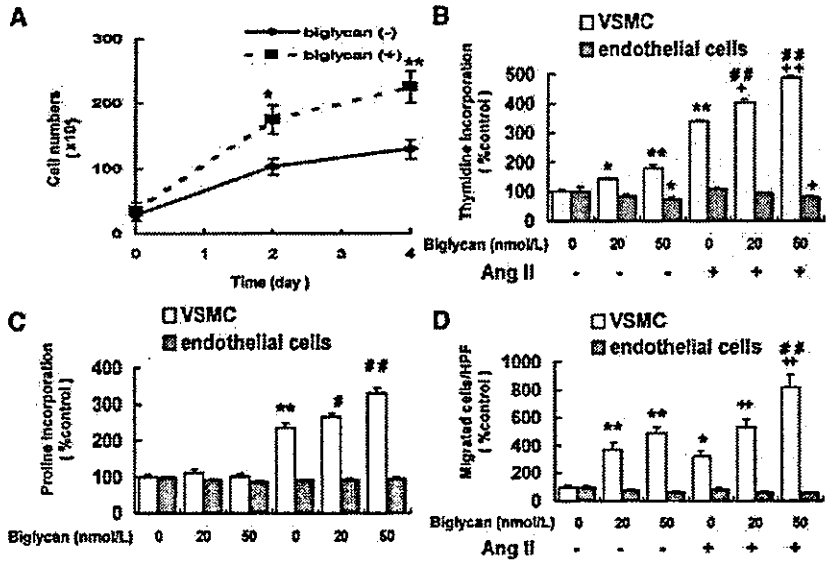

Figure 7. Effects of biglycan and Ang II on cell numbers (A), thymidine incorporation (B), collagen synthesis (C), and cell migration (D) in VSMCs and endothelial cells. *P<0.05, **P<0.01 vs biglycan (−), Ang II (−); +P<0.05, ++P<0.01 vs biglycan (−), Ang II (+): #P<0.05, ##P<0.01 vs corresponding values for biglycan (+), Ang II (−) (n=4).

lar disease, instead of being solely a secondary response to vascular injury. It is well known that susceptibility to vascular stenosis or atherosclerosis differs markedly between individuals and between different arteries within the same individual. The hypothesis that differences in biglycan expression may account for some of these differences requires investigation. Similarly, our observation that the effects of biglycan on cell growth depends on the cell type may be useful not only for understanding the mechanisms of growth regulation of vascular cells in the presence of different types of extracellular matrix, but also may be of future benefit for designing strategies for accelerating the proliferation of one type of cell over another.

In summary, we have shown that overexpression of the extracellular matrix proteoglycan biglycan in the blood vessel to levels similar to those found in diseased arteries results in an increase in vascular hypertrophy, proliferation, and a heightened susceptibility of the coronary arteries to Ang

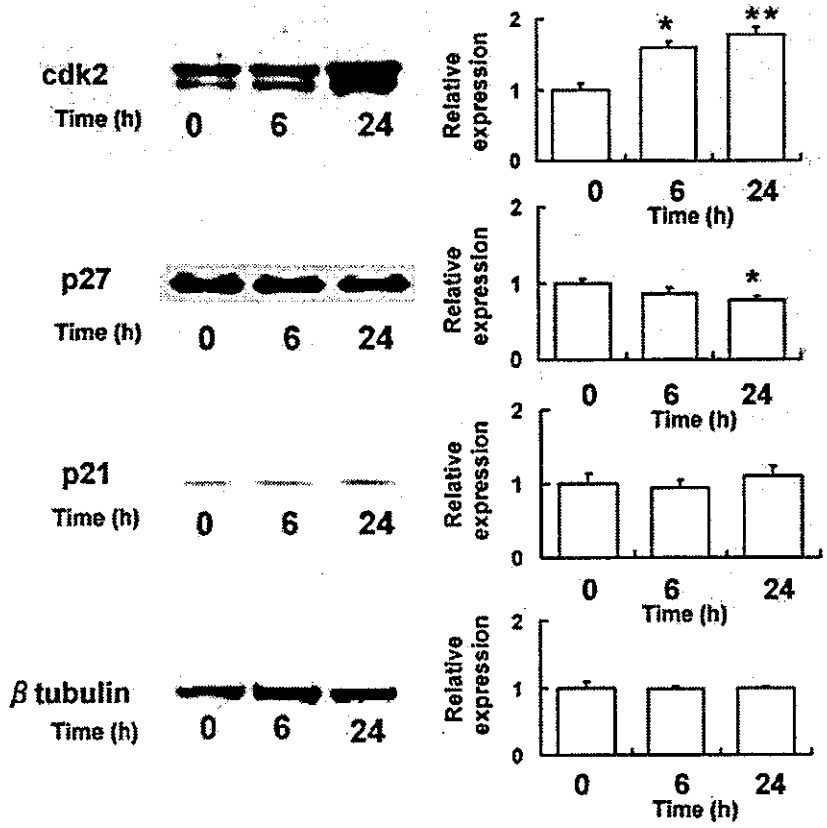

Figure 8. Effect of biglycan (50 nmol/L) on cdk2 kinase (A), p27 (B), p21 (C), and β-tubulin (D) levels in VSMCs. Left, Representative Western blot. Right, Results of densitometric analysis. Densitometric data were normalized to β-tubulin and expressed as relative levels compared with control (0 hour). *P<0.05, **P<0.01 vs control (n=4).

II–induced vascular injury and perivascular fibrosis. These effects may be mediated at least in part by changes in cell cycle–regulatory proteins. These results reinforce the concept that molecules in the extracellular matrix can affect the behavior of the surrounding smooth muscle cells and may have important implications for our understanding of the processes influencing vascular injury.

Acknowledgments

This study was supported by grants from the Ministry of Science and Education, Japan. The authors are grateful to Dr Tomomi Meguro in the laboratory of Dr Tsutomu Yoshikawa, Division of Cardiology, Department of Internal Medicine, School of Medicine, Keio University, for echocardiographic examination of the transgenic mice and to Dr Tatsuo Shimosawa, Department of Nephrology, University of Tokyo, for helpful comments and advice.

References

1. Iozzo RV. Matrix proteoglycans: from molecular design to cellular function. *Annu Rev Biochem.* 1998;67:609–652.
2. Fisher LW, Termine JD, Young MF. Deduced protein sequence of bone small proteoglycan I (biglycan) shows homology with proteoglycan II (decorin) and several nonconnective tissue proteins in a variety of species. *J Biol Chem.* 1989;264:4571–4576.
3. Hocking AM, Shinomura T, McQuillan DJ. Leucine-rich repeat glycoproteins of the extracellular matrix. *Matrix Biol.* 1998;17:1–19.
4. Shimizu-Hirota R, Sasamura H, Mifune M, Nakaya H, Kuroda M, Hayashi M, Saruta T. Regulation of vascular proteoglycan synthesis by angiotensin II type 1 and type 2 receptors. *J Am Soc Nephrol.* 2001;12: 2609–2615.
5. Sasamura H, Shimizu-Hirota R, Nakaya H, Saruta T. Effects of AT1 receptor antagonist on proteoglycan gene expression in hypertensive rats. *Hypertens Res.* 2001;24:165–172.
6. Kuroda M, Sasamura H, Shimizu-Hirota R, Mifune M, Nakaya H, Kobayashi E, Hayashi M, Saruta T. Glucocorticoid regulation of proteoglycan synthesis in mesangial cells. *Kidney Int.* 2002;62:780–789.
7. Kunjathoor VV, Chiu DS, O'Brien KD, LeBoeuf RC. Accumulation of biglycan and perlecan, but not versican, in lesions of murine models of atherosclerosis. *Arterioscler Thromb Vasc Biol.* 2002;22:462–468.
8. Yamakawa T, Bai HZ, Masuda J, Sawa Y, Shirakura R, Ogata J, Matsuda H. Differential expression of proteoglycans biglycan and decorin during neointima formation after stent implantation in normal and atherosclerotic rabbit aortas. *Atherosclerosis.* 2000;152:287–297.
9. O'Brien KD, Olin KL, Alpers CE, Chiu W, Ferguson M, Hudkins K, Wight TN, Chait A. Comparison of apolipoprotein and proteoglycan deposits in human coronary atherosclerotic plaques: colocalization of biglycan with apolipoproteins. *Circulation.* 1998;98:519–527.
10. Riessen R, Isner JM, Blessing E, Loushin C, Nikol S, Wight TN. Regional differences in the distribution of the proteoglycans biglycan and decorin in the extracellular matrix of atherosclerotic and restenotic human coronary arteries. *Am J Pathol.* 1994;144:962–974.
11. Nakano Y, Nishihara T, Sasayama S, Miwa T, Kamada S, Kakunaga T. Transcriptional regulatory elements in the 5′ upstream and first intron regions of the human smooth muscle (aortic type) α-actin-encoding gene. *Gene.* 1991;99:285–289.
12. Li J, Schwimmbeck PL, Tschope C, Leschka S, Husmann L, Rutschow S, Reichenbach F, Noutsias M, Kobalz U, Poller W, Spillmann F, Zeichhardt H, Schultheiss HP, Pauschinger M. Collagen degradation in a murine myocarditis model: relevance of matrix metalloproteinase in association with inflammatory induction. *Cardiovasc Res.* 2002;56:235–247.
13. Susic D, Francischetti A, Frohlich ED. Prolonged L-arginine on cardiovascular mass and myocardial hemodynamics and collagen in aged spontaneously hypertensive rats and normal rats. *Hypertension.* 1999;33: 451–455.
14. Mifune M, Sasamura H, Shimizu-Hirota R, Miyazaki H, Saruta T. Angiotensin II type 2 receptors stimulate collagen synthesis in cultured vascular smooth muscle cells. *Hypertension.* 2000;36:845–850.
15. Nozawa Y, Matsuura N, Miyake H, Yamada S, Kimura R. Effects of TH-142177 on angiotensin II-induced proliferation, migration and intracellular signaling in vascular smooth muscle cells and on neointimal thickening after balloon injury. *Life Sci.* 1999;64:2061–2070.
16. Hildebrand A, Romaris M, Rasmussen LM, Heinegard D, Twardzik DR, Border WA, Ruoslahti E. Interaction of the small interstitial proteoglycans biglycan, decorin and fibromodulin with transforming growth factor β. *Biochem J.* 1994;302(pt 2):527–534.
17. Kolb M, Margetts PJ, Sime PJ, Gauldie J. Proteoglycans decorin and biglycan differentially modulate TGF-β-mediated fibrotic responses in the lung. *Am J Physiol Lung Cell Mol Physiol.* 2001;280:L1327–L1334.
18. Schonherr E, Witsch-Prehm P, Harrach B, Robenek H, Rauterberg J, Kresse H. Interaction of biglycan with type I collagen. *J Biol Chem.* 1995;270:2776–2783.
19. Wiberg C, Heinegard D, Wenglen C, Timpl R, Morgelin M. Biglycan organizes collagen VI into hexagonal-like networks resembling tissue structures. *J Biol Chem.* 2002;277:49120–49126.
20. Ameye L, Aria D, Jepsen K, Oldberg A, Xu T, Young MF. Abnormal collagen fibrils in tendons of biglycan/fibromodulin-deficient mice lead to gait impairment, ectopic ossification, and osteoarthritis. *FASEB J.* 2002;16:673–680.
21. Xu T, Bianco P, Fisher LW, Longenecker G, Smith E, Goldstein S, Bonadio J, Boskey A, Heegaard AM, Sommer B, Satomura K, Dominguez P, Zhao C, Kulkarni AB, Robey PG, Young MF. Targeted disruption of the biglycan gene leads to an osteoporosis-like phenotype in mice. *Nat Genet.* 1998;20:78–82.
22. Shirk RA, Parthasarathy N, San Antonio JD, Church FC, Wagner WD. Altered dermatan sulfate structure and reduced heparin cofactor II-stimulating activity of biglycan and decorin from human atherosclerotic plaque. *J Biol Chem.* 2000;275:18085–18092.
23. Stokes MB, Holler S, Cui Y, Hudkins KL, Eitner F, Fogo A, Alpers CE. Expression of decorin, biglycan, and collagen type I in human renal fibrosing disease. *Kidney Int.* 2000;57:487–498.
24. Lin H, Wilson JE, Roberts CR, Horley KJ, Winters GL, Costanzo MR, McManus BM. Biglycan, decorin, and versican protein expression patterns in coronary arteriopathy of human cardiac allograft: distinctness as compared to native atherosclerosis. *J Heart Lung Transplant.* 1996; 15:1233–1247.
25. Hengst L, Reed SI. Translational control of p27Kip1 accumulation during the cell cycle. *Science.* 1996;271:1861–1864.
26. Boehm M, Nabel EG. Cell cycle and cell migration: new pieces to the puzzle. *Circulation.* 2001;103:2879–2881.
27. Weber CK, Sommer G, Michl P, Fensterer H, Weimer M, Gansauge F, Leder G, Adler G, Gress TM. Biglycan is overexpressed in pancreatic cancer and induces G1-arrest in pancreatic cancer cell lines. *Gastroenterology.* 2001;121:657–667.
28. Kikuchi A, Tomoyasu H, Kido I, Takahashi K, Tanaka A, Nonaka I, Iwakami N, Kamo I. Haemopoietic biglycan produced by brain cells stimulates growth of microglial cells. *J Neuroimmunol.* 2000;106:78–86.
29. Schaefer L, Beck KF, Raslik I, Walpen S, Mihalik D, Micegova M, Macakova K, Schonherr E, Seidler DG, Varga G, Schaefer RM, Kresse H, Pfeilschifter J. Biglycan, a nitric oxide-regulated gene, affects adhesion, growth and survival of mesangial cells. *J Biol Chem.* 2003; 278:26227–26237.
30. Fischer JW, Kinsella MG, Levkau B, Clowes AW, Wight TN. Retroviral overexpression of decorin differentially affects the response of arterial smooth muscle cells to growth factors. *Arterioscler Thromb Vasc Biol.* 2001;21:777–784.
31. Schonherr E, Levkau B, Schaefer L, Kresse H, Walsh K. Decorin-mediated signal transduction in endothelial cells. Involvement of Akt/protein kinase B in up-regulation of p21(WAF1/CIP1) but not p27(KIP1). *J Biol Chem.* 2001;276:40687–40692.
32. Fischer JW, Kinsella MG, Clowes MM, Lara S, Clowes AW, Wight TN. Local expression of bovine decorin by cell-mediated gene transfer reduces neointimal formation after balloon injury in rats. *Circ Res.* 2000; 86:676–683.
33. Giri SN, Hyde DM, Braun RK, Gaarde W, Harper JR, Pierschbacher MD. Antifibrotic effect of decorin in a bleomycin hamster model of lung fibrosis. *Biochem Pharmacol.* 1997;54:1205–1216.
34. Border WA, Noble NA, Yamamoto T, Harper JR, Yamaguchi Y, Pierschbacher MD, Ruoslahti E. Natural inhibitor of transforming growth factor-β protects against scarring in experimental kidney disease. *Nature.* 1992;360:361–364.

Human mesenchymal stem cells in rodent whole-embryo culture are reprogrammed to contribute to kidney tissues

Takashi Yokoo*†‡, Toya Ohashi†§, Jin Song Shen†, Ken Sakurai†§, Yoichi Miyazaki*†, Yasunori Utsunomiya*, Masanori Takahashi¶, Yoshio Terada‖, Yoshikatsu Eto†§, Tetsuya Kawamura*, Noriko Osumi¶, and Tatsuo Hosoya*

Departments of *Internal Medicine and Gene Therapy and §Pediatrics, †Institute of DNA Medicine, Jikei University School of Medicine, 3-25-8, Nishi-shimbashi, Minato-ku, Tokyo 105-8461, Japan; ¶Division of Developmental Neuroscience, Tohoku University Graduate School of Medicine, 2-1, Seiryo-machi, Aoba-ku, Sendai 980-8575, Japan; and ‖Department of Homeostasis Medicine and Nephrology, Tokyo Medical and Dental University, 5-45 Yushima 1-chome, Bunkyo-ku, Tokyo 113-8519, Japan

Edited by Erkki Ruoslahti, The Burnham Institute, La Jolla, CA, and approved January 4, 2005 (received for review September 16, 2004)

The use of stem cells has enabled the successful generation of simple organs. However, anatomically complicated organs such as the kidney have proven more refractory to stem-cell-based regenerative techniques. Given the limits of allogenic organ transplantation, an ultimate therapeutic solution is to establish self-organs from autologous stem cells and transplant them as syngrafts back into donor patients. To this end, we have striven to establish an *in vitro* organ factory to build up complex organ structures from autologous adult stem cells by using the kidney as a target organ. Cultivation of human mesenchymal stem cells in growing rodent embryos enables their differentiation within a spatially and temporally appropriate developmental milieu, facilitating the first step of nephrogenesis. We show that a combination of whole-embryo culture, followed by organ culture, encourages exogenous human mesenchymal stem cells to differentiate and contribute to functional complex structures of the new kidney.

organogenesis | regeneration

Organ regeneration has recently attracted considerable attention as a new therapeutic strategy. The potential for regenerative medicine has been gradually realized with the discovery of tissue stem cells and the reported therapeutic benefits of their implantation or systemic delivery for the regeneration of several tissues such as neurons (1), β-islet cells (2), myocytes (3) and vessels (4). However, success using such strategies to date has been limited to cells and simple tissues. Anatomically complicated organs such as the kidney and lung, which are comprised of several different cell types and have a sophisticated 3-dimensional organization and cellular communication, have proven more refractory to stem cell-based regenerative techniques. Allogenic tissue transplantation by using a scaffold is an alternative strategy to replace whole organs. However, the scarcity of suitable organs has prevented organ transplantation from becoming a practical solution in most cases of organ failure. Furthermore, chronic rejection of the allograft remains a common cause of graft failure after organ transplantation despite life-long administration of immunosuppressive agents (5). One of the ultimate therapeutic aims is therefore to establish self-organs from autologous tissue stem cells and transplant the *in vitro*-derived organ as a syngraft back into the donor individual.

Human mesenchymal stem cells (hMSCs) found in adult bone marrow were recently shown to maintain plasticity and to differentiate into several different cell types, depending on their microenvironment (6). In contrast to embryonic stem cells, adult MSCs can be isolated from autologous bone marrow and applied for therapeutic use without any serious ethical issues or immunologic consequences (7). Primary hMSCs were obtained from the bone marrow of healthy volunteers and used throughout this study.

The kidney was selected as the target organ for this study, because it represents a complicated organ, comprising several different cell types, has a sophisticated 3D organization, and its embryonic development has been well researched. Kidney development is initiated when the metanephric mesenchyme at the caudal portion of the nephrogenic cord (8) induces the nearby Wolffian duct to produce a ureteric bud (9). Development proceeds as a result of reciprocal epithelial-mesenchymal signaling between the ureteric bud and metanephric mesenchyme (10). To test whether hMSCs could participate in kidney development, they were initially cocultured with either rodent Wolffian duct extracted at the embryonic stage immediately before formation of the kidney primordia, or with established metanephric rudiment. However, this procedure was not sufficient to achieve kidney organogenesis or even integration of hMSCs into the developing rodent metanephros (T.Y., unpublished data). This finding suggests that hMSCs must be placed in a specific, defined embryonic niche to allow for exposure to the repertoire of nephrogenic signals required to generate the organ. This outcome can best be achieved by implanting hMSCs into the nephrogenic site of a developing embryo. However, it is difficult to implant cells prenatally at the exact site of organogenesis by a transuterus approach. Equally, once embryos are removed for cell implantation, they cannot be returned to the uterus for further development. Therefore, embryos were isolated from uteri for cell implantation, after which they were further developed *in vitro*, using whole-embryo culture. Here, we show that by using this culture combination, hMSCs develop into morphologically identical cells to endogenous renal cells and are able to contribute to complex kidney structures.

Methods

Animals. Wild-type Sprague–Dawley rats were purchased from Sankyo Lab Services (Tokyo). A breeding colony of Fabry mice was established at the Laboratory Animal Center of the Jikei University School of Medicine from breeding pairs that were kindly donated by R. O. Brady (National Institutes of Health, Bethesda). The midpoint on the day when a vaginal plug was observed was designated as day 0.5. Animals were housed in a ventilated (positive airflow) rack and bred and maintained under pathogen-free conditions. All experimental procedures were

This paper was submitted directly (Track II) to the PNAS office.

Abbreviations: hMSC, human mesenchymal stem cell; GDNF, glial cell line-derived neurotrophic factor; En, embryonic day n; α-gal A, α-galactosidase A; Gb3, globotriaosylceramide; AQP-1, aquaporin-1; PTH, parathyroid hormone; NBC-1, Na^+-HCO_3^- cotransporter 1; GLEPP-1, glomerular epithelial protein 1; DiI, 1,1′-dioctadecyl-3,3,3′,3′-tetramethylindocarbocyanine.

‡To whom correspondence should be addressed. E-mail: tyokoo@jikei.ac.jp.

www.pnas.org/cgi/doi/10.1073/pnas.0406878102

approved by The Committee for Animal Experiments of the Jikei University School of Medicine.

Culture and Manipulation of hMSCs. Bone marrow-derived hMSCs that were confirmed to be CD105-, CD166-, CD29-, and CD44-positive and CD14-, CD34-, and CD45-negative, were purchased from Cambrex Bio Science Walkersville (Walkersville, MD) and cultured according to the manufacturer's instructions. The hMSCs were used within five cell passages to avoid phenotypic changes. A replication-defective recombinant adenovirus carrying human glial cell line-derived neurotrophic factor (GDNF) cDNA (AxCAhGDNF) was generated and purified as described (11). Packaging cells (ψ-crip) that produce a recombinant retrovirus bearing the bacterial LacZ gene, MFG-LacZ, were a gift from H. Hamada (Sapporo Medical University, Sapporo, Japan). Adenoviral and retroviral infection were performed as described (12, 13). The cells were labeled with 1,1'-dioctadecyl-3,3,3',3'-tetramethylindocarbocyanine (DiI) (Molecular Probes) at 0.25% (wt/vol) in 100% dimethylformamide and injected by using micropipettes at the site of ureteric bud sprouting.

Whole-Embryo Culture and Organ Culture. Whole embryos were cultured *in vitro* according to a method described (14), with several modifications. Using a surgical microscope at low-power magnification, uteri were dissected from anaesthetized mothers. Stage embryonic day (E)11.5 rat embryos and stage E9.5 mouse embryos were freed from the uterine wall, decidua, and the outer-membrane layer, including Reichert's membrane. The yolk sac and amnion were opened to enable injection but the chorioallantoic placenta was left intact. Successfully injected embryos were immediately cultivated in 15-ml culture bottles containing 3 ml of culture media consisting of 100% centrifuged rat serum supplemented with glucose (10 mg/ml), penicillin G (100 units/ml), streptomycin (100 μg/ml), and amphotericin B (0.25 μg/ml). The culture bottles were allowed to rotate in an incubator (model no. RKI10–0310, Ikemoto, Tokyo). *Ex vivo* development of the rat embryos was assessed after 24- and 48-h cultivation periods and compared with E12.5 and E13.5 rat embryos. Forty-eight hours later, embryos were assessed for heartbeat, whole-body blood circulation, and general morphology. Kidney rudiments were dissected and cultured as described (15). To enhance the accumulation of globotriaosylceramide (Gb3) in the kidney primordia, the cultivated metanephroi were cultured in the presence of ceramide trihexoside (1 nmol, Sigma) (16). α-galactosidase A (α-gal A) enzymatic activity in metanephroi was fluorometrically assessed as described (17).

Histology. Two-color staining of metanephroi were performed essentially as described (17) by using mouse anti-β-gal (Promega) and rabbit anti-human WT-1 (Santa Cruz Biotechnology) as the primary antibodies. A monoclonal mouse anti-Gb3 antibody (Seikagaku, Tokyo) was also used. Whole-mount *in situ* hybridization with digoxigenin UTP-labeled *c-ret* riboprobes was performed as described (15). *In situ* hybridization was also performed on histological sections by using biotin-labeled human genomic *Alu*I/II probes (Invitrogen) according to the manufacturer's protocol. An X-gal assay was used to assess expression of the LacZ gene as described (13).

Identification of hMSC-Positive Cells. Metanephroi generated by relay culture were digested in collagenase type I (1 mg/ml) for 30 min and labeled with fluorescein digalactoside (Molecular Probes) by using transient permeabilization by hypotonic shock as described by Fiering *et al.* (18) (FACS-galactosidase assay). LacZ-positive cells were sorted by using a cell sorter (Becton Dickinson). Total RNA was extracted and subjected to RT-PCR to analyze expression of aquaporin-1 (AQP-1), parathyroid hormone (PTH) receptor 1, 1α hydroxylase, Na^+-HCO_3^- cotransporter 1 (NBC-1), nephrin, podocine, and glomerular epithelial protein 1 (GLEPP-1). A list of primer sequences and reaction conditions used can be found in Table 1, which is published as supporting information on the PNAS web site. For the analysis of cell ploidy, cells were stained with propidium iodide, and DNA content was assessed by using a flow cytometer.

Statistical Analysis. Data were expressed as the mean ± SE. Statistical analysis was performed by using the two-sample t test to compare data in different groups. $P < 0.05$ was taken to be statistically significant.

Results and Discussion

The whole-embryo culture system was first optimized to allow a defined concentration of oxygen to be supplied continuously to rotating culture bottles, thus improving embryonic development *ex utero* (14). Using this system, rat embryos (E11.5), together with the yolk sac, amnion, and chorioallantoic placenta were cultured in the media consisting of 100% freshly centrifuged rat serum supplemented with glucose (10 mg/ml) at 37°C in the culture bottle (see Movie 1, which is published as supporting information on the PNAS web site). Forty-eight hours later, embryos were assessed for heartbeat, whole-body blood circulation, and general morphology. Based on the resultant somite number and general morphology, the devel-

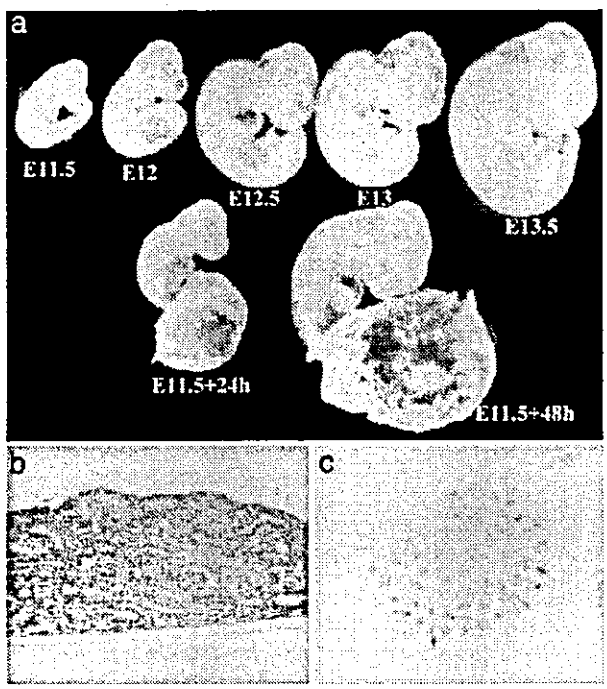

Fig. 1. *Ex utero* development of kidney primordia by using the relay culture system. Rat embryos (E11.5) just before ureteric bud sprouting were cultured *in vitro*, using a whole-embryo culture system for 48 h. After 24 and 48 h in culture, *ex utero* development of the rat embryos was assessed by comparing them with those that had grown in the uterus for E11.5, E12.0, E12.5, E13.0 and E13.5. Embryos that were developed in the culture bottle reached stages of development that were consistent with E13 embryos that had developed *in utero*. (*a*). At the end of the 48-h culture period, kidney rudiments were isolated and subjected to metanephric organ culturing for 6 days. To confirm the extent of tubulogenesis and ureteric bud branching, hematoxylin/eosin staining (*b*) and whole-mount *in situ* hybridization for *c-ret* (*c*) were performed. Fine tubulogenesis and ureteric bud branching can be observed. Experiments were performed in triplicate and representative pictures are shown.

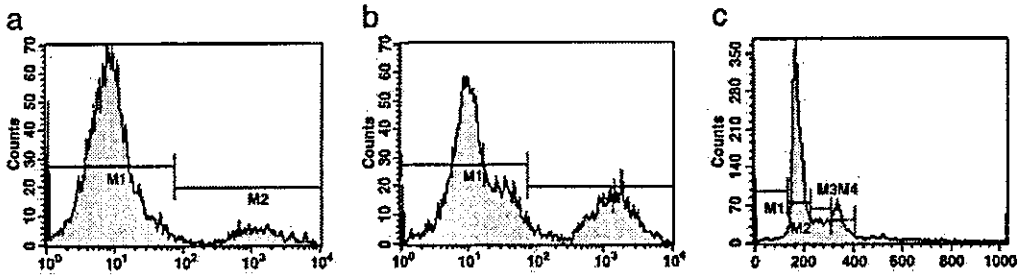

Fig. 2. Proportion of donor-derived cells in culture-derived metanephroi and assessment of their DNA ploidy. hMSCs expressing the LacZ gene were retrovirally transfected with GDNF (*b*) or without GDNF (*a*) and injected into rodent embryos at the site of budding. After relay culture, the neogenerated metanephroi were digested with collagenase, and single cells were subjected to a FACS-galactosidase assay. M, the informative peak. The use of GDNF was found to significantly increase the number of hMSCs that were incorporated into the developing metanephroi. (*c*) LacZ-positive cells were sorted, and their DNA content was assessed by using propidium iodide intensity. These cells were found to be euploid, and thus did not represent transplanted hMSCs that had fused with host metanephric cells. Ten thousand cells were subjected to flow cytometric analysis. Experiments were performed in quadruplicate and representative figures are shown.

opmental age of rat embryos cultured in this way appeared consistent with E13 embryos that had developed *in utero* (Fig. 1*a*). At this stage, ureteric buds were elongated and initial branching was completed (data not shown), indicating that during culture, the metanephric mesenchyme had been stimulated to undertake the initial step of commitment toward nephrogenesis. However, embryos could not develop further and died soon after 48 h because of insufficient development of the placenta *in vitro* (19). To overcome this limitation, whole-embryo culture was followed by organ culture. After whole-embryo culture for 48 h, metanephroi were dissected from embryos and subjected to organ culture for 6 days. Using this combination, which will be referred to as relay culture, kidney rudiments continued to grow *in vitro*, as assessed by the observation of fine tubulogenesis and ureteric bud branching (Fig. 1 *b* and *c*). Thus, the metanephros can complete devel-

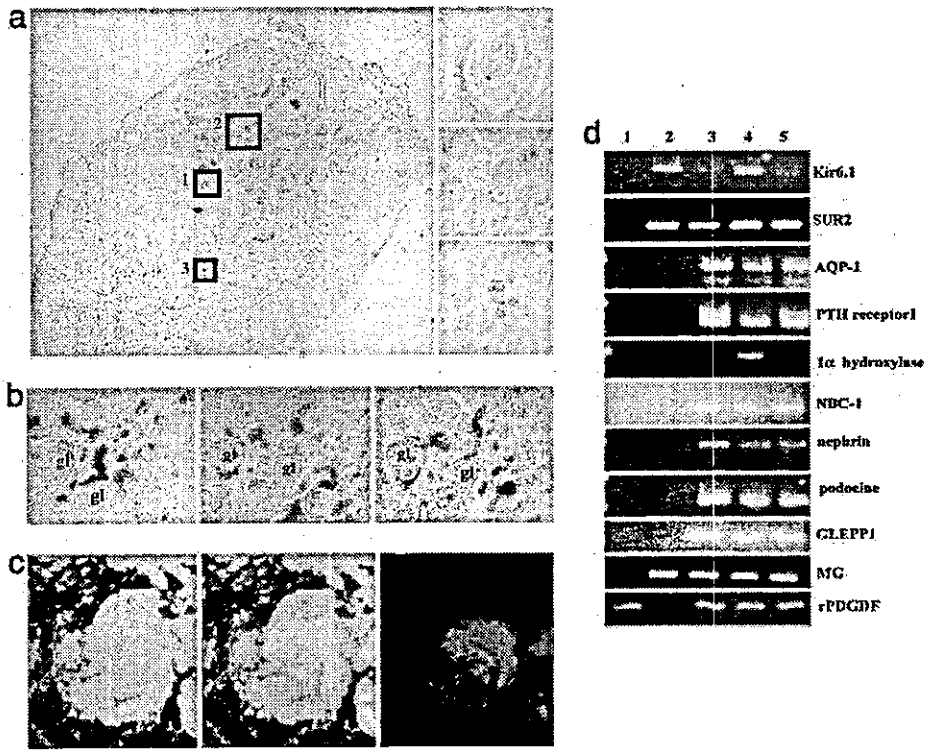

Fig. 3. Differentiation of transplanted hMSCs into organized, resident renal cells. (a) After relay culturing, the resulting metanephros was subjected to an X-gal assay to trace the transplanted hMSCs. The morphology of these LacZ-positive cells (shown under high magnification; ×400) and the renal structures to which they contributed, were consistent with them being glomerular epithelial cells (lane 1), tubular epithelial cells (lane 2), and interstitial cells (lane 3). (*b*) Serial sections were examined by light microscopy. Glomerular epithelial cells were linked to tubular epithelial cells (arrow head), and some of these cells formed a continuous tubular extension toward the medulla (arrow). gl, glomerulus. (*c*) Tissue sections were subjected to two-color immunofluorescent staining for β-gal (*Left*) and WT-1 (*Right*). (*Center*) A merged image is presented. (*d*) After relay culture, the resulting metanephroi were digested, and single cells were subjected to the FACS-galactosidase assay. LacZ-positive cells were sorted and subjected to RT-PCR for expression analysis of Kir6.1, SUR2, AQP-1, PTH receptor 1, 1α hydroxylase, NBC-1, nephrin, podocin, GLEPP1, human-specific β_2 microgloblin (MG) and rat GAPDH. Lane 1, control rat metanephros; lane 2, hMSCs; lanes 3–5, regenerated metanephros from three individual experiments. Representative photographs are shown.

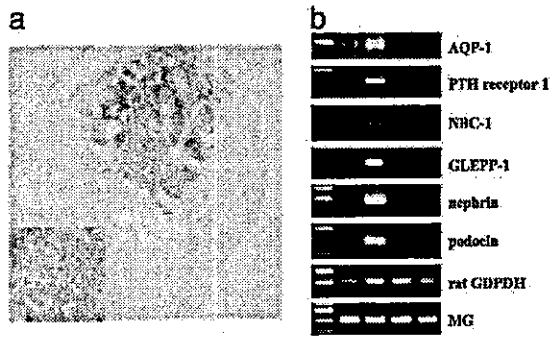

Fig. 4. Injection and culture of hMSCs in isolated metanephroi. hMSCs expressing the LacZ gene were retrovirally transfected with GDNF and injected into the cultured metanephroi (E13). (*a*) After 6 days of organ culture, the resulting metanephroi were subjected to an X-gal assay. (*Inset*) LacZ-positive cells at a high magnification are shown. Note that hMSCs-derived cells remain aggregated and do not form recognizable kidney structures. (*b*) RNAs were extracted and subjected to RT-PCR. Neogenerated kidney rudiment before (lane 2) and after (lane 3) organ culturing is shown. Mixture of metanephroi and hMSCs before (lane 4) and after (lane 5) organ culture is shown. Note that only the hMSCs differentiated in the whole embryo are able to express kidney-specific gene after organ culture. Lane 1, maker (ϕX174/*Hae*III).

opment *ex utero*, even if the embryo is dissected before the stage at which the ureteric bud sprouts.

Using this system, hMSCs were injected into rodent embryos at the site of organogenesis. To distinguish the donor-derived cells from host cells, hMSCs were labeled with the LacZ gene and DiI. A total of 1×10^3/embryo of labeled cells were then injected into the intermediate mesoderm between the somite and the lateral plate at the level of somite 29 for rat and somite 26 for mouse, which we previously estimated by *in situ* hybridization for *c-ret*, to be the ureteric budding sites (15). Successful injection was confirmed by *in situ* hybridization for human genomic *Alu*I/II, which identifies exclusively human cells, and injected hMSCs-derived cells were detected along the Wolffian duct (see Fig. 6, which is published as supporting information on the PNAS web site). After relay culture, LacZ-positive cells were detected in the metanephros (5.0 ± 4.2%), as measured by a FACS-galactoside assay of single cells derived from a dissected metanephros (Fig. 2*a*). No LacZ-positive cells were detected in the isolated kidney if the injection site was altered by >1 somite in length. In control embryos, injection of labeled mouse fibroblasts instead of hMSCs resulted in only a negligible number of LacZ-positive cells detected in the metanephros (data not shown). To enhance the number of integrated donor-derived cells, the hMSCs were further modified before injection to temporally express GDNF by using the adenovirus AxCAh-GDNF (11). GDNF is normally expressed in metanephric mesenchyme at this stage, and the interaction between GDNF and its receptor, c-ret, is required for epithelial-mesenchymal signaling to occur (10). The FACS-galactosidase assay revealed a significant increase in the number of LacZ-positive cells that were detected after transient GDNF expression (29.8 ± 9.2%, Fig. 2*b*). Importantly, 68.8 ± 11.4% of LacZ-positive cells in the neogenerated metanephros were euploid (Fig. 2*c*). The number of LacZ-positive cells were significantly increased ($2.84 \pm 0.49 \times 10^5$/metanephros) compared with the starting number of injected cells (1×10^3/embryo), suggesting that the remaining polyploid cells were mostly undergoing cell division. Furthermore, FISH, using the human and rat Y chromosome showed that a negligible number of cells were doubly positive for the Y chromosome (≈0.1%, see Fig. 7, which is published as supporting information on the PNAS web site). These data strongly suggest that, if any, only a small percentage of hMSC cells undergo cell fusion during differentiation.

During metanephric organ culture, DiI-positive cells migrated toward the medulla and dispersed in the kidney primordia (see Fig. 8, which is published as supporting information on the PNAS web site), suggesting that the transplanted cells become integrated in the host kidney. To confirm that these cells contribute to renal structures, the kidney primordia was subjected to an X-gal assay. LacZ-positive cells were scattered throughout the metanephric rudiment and were morphologically identical to the resident glomerular epithelial cells, tubular epithelial cells, and interstitial cells (Fig. 3*a*). Serial sections of metanephric rudiment showed glomerular epithelial cells linked to tubular epithelial cells (Fig. 3*b*, arrowhead). Some β-gal-positive cells of the S-shaped bodies were also positive for WT-1, which is strongly expressed in glomerular podocytes at this stage (20) (Fig. 3*c*). RT-PCR of FACS-sorted metanephric cells revealed that LacZ-positive cells expressed podocyte-specific genes (nephrin, podocine, and GLEPP-1) and tubular epithelial cell-specific genes (AQP-1, 1α hydroxylase, PTH receptor 1, and NBC-1) (Fig. 3*d*). In contrast to endogenous renal cells, ATP-sensitive K^+ channel subunit, Kir6.1/SUR2 (21), which is expressed in hMSCs, was still expressed after relay culture. Furthermore, when hMSCs were injected into cultured metanephroi (E13), cell dispersal was not observed, and the hMSCs remained aggregated. After 6 days in organ culture, the hMSCs failed to contribute to kidney structures (Fig. 4*a*), and did not express kidney-specific genes (Fig. 4*b*). These data suggest that during whole-embryo culture, hMSCs complete an initial step essential for commitment to a renal fate and that during organ culture, they further undergo a mesenchyme-to-epithelium transition or stromogenic differentiation.

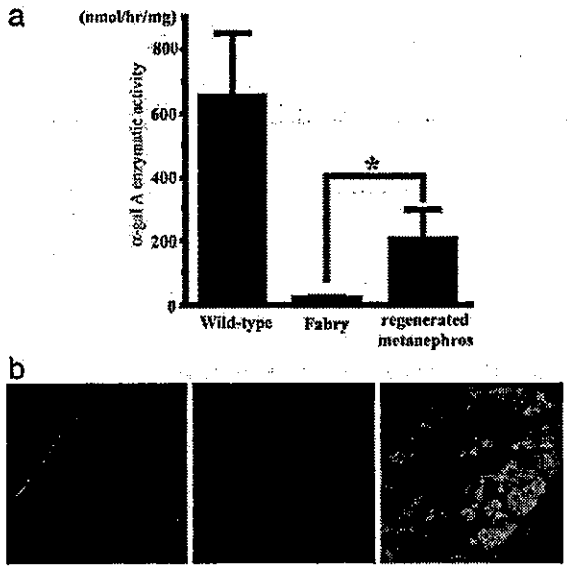

Fig. 5. Therapeutic kidney regeneration in an α-Gal A-null Fabry mouse. hMSCs were transplanted into E9.5 embryos of Fabry mice lacking the α-gal A gene and subjected to relay culture. (*a*) The α-gal A enzymatic bioactivity of resulting metanephroi was fluorometrically assessed as described (19). For the controls, metanephros from wild-type mice (*Left*) and Fabry mice (*Right*) were also subjected to the same protocol. The data are shown as the means ± SE. Asterisks indicate statistically significant differences ($P < 0.05$) between the two groups. (*b*) To confirm the potency of Gb3 clearance in resulting metanephroi, organ culture was performed in the presence of Gb3, and accumulation in the metanephroi was assessed by immunostaining for Gb3. Control metanephroi from wild-type mice (*Left*) and Fabry mice (*Right*) were subjected to the same analysis.

CELL BIOLOGY